1 **Contemporary human H3N2 influenza A viruses require a low**

2 **threshold of suitable glycan receptors for efficient infection**

3 Cindy M. Spruit[1], Igor R. Sweet[1], Theo Bestebroer[2], Pascal Lexmond[2], Boning Qiu[3],

4 Mirjam J.A. Damen[4], Ron A. M. Fouchier[2], Joost Snijder[4], Sander Herfst[2], Geert-Jan

5 Boons[1,5], Robert P. de Vries[1*]

6 [1]   Department of Chemical Biology & Drug Discovery, Utrecht Institute for

7 Pharmaceutical Sciences, Utrecht University, Universiteitsweg 99, 3584CG, Utrecht,

8 The Netherlands

9 [2]   Department of Viroscience, Erasmus University Medical Center, Dr.

10 Molewaterplein 50, 3015GE Rotterdam, The Netherlands

11 [3]   Department of Pharmaceutics, Utrecht Institute for Pharmaceutical Sciences,

12 Utrecht University, Universiteitsweg 99, 3584 CG Utrecht, The Netherlands

13 [4]   Biomolecular Mass Spectrometry and Proteomics, Bijvoet Center for

14 Biomolecular Research and Utrecht Institute of Pharmaceutical Sciences, Utrecht

15 University, Padualaan 8, 3584CH, Utrecht, The Netherlands

16 [5]   Complex Carbohydrate Research Center, University of Georgia, 315 Riverbend

17 Rd, Athens, GA 30602, USA

18

19 [*] for correspondence: r.vries@uu.nl

Abstract

Recent human H3N2 influenza A viruses (IAV) have evolved to employ elongated glycans terminating in α2,6-linked sialic acid as their receptors. These glycans are displayed in low abundancies by cells commonly employed to propagate these viruses (MDCK and hCK), resulting in low or no viral propagation. Here, we examined whether the overexpression of the glycosyltransferases B3GNT2 and B4GALT1, which are responsible for the elongation of poly-N-acetyllactosamines (LacNAc), would result in improved A/H3N2 propagation. Stable overexpression of B3GNT2 and B4GALT1 in MDCK and hCK cells was achieved by lentiviral integration and subsequent antibiotic selection and confirmed by qPCR and protein mass spectrometry experiments. Flow cytometry and glycan mass spectrometry experiments using the B3GNT2 and/or B4GALT1 knock-in cells demonstrated increased binding of viral hemagglutinins and the presence of a larger number of LacNAc repeating units, especially on hCK-B3GNT2 cells. An increase in the number of glycan receptors did, however, not result in a greater infection efficiency of recent human H3N2 viruses. Based on these results, we propose that H3N2 IAVs require a low number of suitable glycan receptors to infect cells and that an increase in the glycan receptor display above this threshold does not result in improved infection efficiency.

Introduction

Influenza A viruses (IAV) of the H3N2 subtype cause seasonal epidemics, leading to illness, hospitalizations, and deaths in humans [1]. The crucial first step of infection is the binding of the viral hemagglutinin (HA) to a receptor on a cell, which are glycans terminating in α2,6-linked sialic acids (SIA) for human IAVs [2, 3]. H3N2 viruses have been circulating in the human population since 1968 and due to continuous immune evasion, antigenic drift of the surface proteins of IAVs takes place. This antigenic drift of H3N2 viruses has changed receptor specificities [4] and recent H3N2 viruses bind to longer glycans having multiple consecutive oligo-N-acetyllactosamine (LacNAc) moieties terminating in an α2,6-linked SIA [2, 4-11]. This specificity is most pronounced for H3N2 viruses of subclade 3C.2a, which require at least three subsequent LacNAc repeating units for binding [12].

These altered receptor specificities make it difficult to isolate and propagate H3N2 viruses, greatly hampering the further study of these viruses [8, 13-16]. Even when virus isolation is successful, viruses may have acquired adaptive mutations in the receptor binding site of HA, especially when isolated in eggs instead of MDCK (Madin-Darby Canine Kidney) cells [13, 15, 17-20]. MDCK cells have previously been modified to produce more α2,6-linked SIAs by the overexpression of the enzyme ST6GAL1, resulting in MDCK-SIAT1 [21] and MDCK-AX4 [22] cells. These cells enabled the isolation of H3N2 viruses, especially of the 3C.2a and 3C.3a subclades, and resulted in higher titers of viral stocks [16, 23]. To allow the isolation of further evolved contemporary H3N2 viruses, with higher titers and fewer mutations, MDCK cells were further modified to eliminate α2,3-linked SIAs while also overexpressing α2,6-linked SIAs, resulting in "humanized" MDCK (hCK) cells [15].

3

62   Analysis of the *N*-glycans of MDCK, MDCK-SIAT1, and hCK cells indicated a low

63   abundance of glycans with at least three successive LacNAc repeating units

64   terminating in an α2,6-linked SIA [24]. The enzyme beta-1,3-N-

65   acetylglucosaminyltransferase (B3GNT2) is responsible for the addition of N-

66   acetylglucosamine to glycans, while the galactose is transferred to the glycan by the

67   enzyme beta-1,4-galactosyltransferase 1 (B4GALT1). Previously, we successfully

68   used these two enzymes to elongate LacNAc repeating units both in chemoenzymatic

69   synthesis [25, 26] and on biological membrane surfaces of erythrocytes [12].

70   Here, we genetically engineered MDCK and hCK cells to overexpress B3GNT2 and

71   B4GALT1 and demonstrated that this resulted in a higher relative abundance of *N*-

72   glycans having elongated LacNAc moieties. Surprisingly, although the

73   B3GNT2/B4GALT1 knock-in cells exhibited elevated binding of recent H3 HAs, the

74   overexpression did not lead to improved virus isolation and infection efficiency.

75   Several studies have indicated that a higher display of appropriate receptors leads to

76   increased infectivity [15, 21, 22, 27], while others indicated that only low amounts of

77   receptors are required for infection [28-30]. Based on our studies, we concluded that

78   above a required threshold, a greater number of suitable glycan receptors for H3N2

79   IAVs does not result in increased infection efficiency.

Results

Generation of stable B3GNT2 and B4GALT1 knock-in MDCK and hCK cell lines

Rearrangement of the sialyltransferase expression in hCK cells supported increased replication of many human H3N2 viruses [15]. However, only small quantities of glycans with multiple LacNAc repeating units appeared to be present on both MDCK and hCK cells [24]. Recently, we and others have shown that poly-LacNAc containing *N*-glycans are critical for the binding of contemporary H3N2 viruses [8, 12]. Therefore, we used the glycosyltransferases B3GNT2 and B4GALT1 to increase the biosynthesis of LacNAc repeating units to produce extended *N*-glycans [12, 25, 26, 31]. We hypothesized that the overexpression of B3GNT2 and/or B4GALT1 in MDCK and hCK cells would produce appropriate glycan receptors for recent H3N2 (subclade 3C.2a) IAVs.

To accomplish the overexpression of these genes in MDCK and hCK cells, lentiviral transfer plasmids encoding the human *B3GNT2* and/or *B4GALT1* genes, together with the *Hygromycin B resistance* gene, were constructed. The genes were expressed from one human EF-1α promoter [32] and separated by P2A (and for double glycosyltransferase knock-ins also T2A) self-cleaving peptides. Lentiviruses were produced with a transfer plasmid and packaging plasmids, after which the viruses were used to transduce MDCK and hCK cells (Fig. 1A). Cells in which the genes were inserted in the genome were selected with Hygromycin B.

Stable overexpression of *B3GNT2* and *B4GALT1* was confirmed by RT-qPCR analysis on isolated cellular RNA. Primers for the *B3GNT2*, *B4GALT1*, and *ST6GAL1* genes were used, and the obtained values were normalized to the reference gene *GAPDH* (Fig. 1B). Overexpression of the control gene *ST6GAL1* was clearly shown in

5

104 hCK but not MDCK cells. Furthermore, the overexpression of *B3GNT2* and *B4GALT1*

105 was present in all cell lines in which these knock-ins were made. It should be noted

106 that expression levels in the double knock-in cell lines showed lower expression of the

107 glycosyltransferases, especially for *B3GNT2* in MDCK-B3GNT2-B4GALT1 cells.

108 Thereafter, the protein levels of B3GNT2, B4GALT1, and ST6GAL1 in cell lysates

109 were measured using proteomic experiments based on liquid chromatography

110 coupled to tandem mass spectrometry, using label-free quantitation relative to tubulin

111 beta expression (Fig. 1C). Only peptides unique for the human B3GNT2, B4GALT1,

112 and ST6GAL1 were selected. The proteomic data is comparable to the RT-qPCR data

113 since elevated protein levels in the cell lines with knock-ins were observed.

114 Collectively, the data showed that the stable overexpression of B3GNT2 and

115 B4GALT1 in MDCK and hCK was successful.

116 **Flow cytometric characterization of B3GNT2 and B4GALT1 knock-in cells with**

117 **plant and viral lectins**

118 Next attention was focused on whether the overexpression of B3GNT2 and/or

119 B4GALT1 led to a display of a higher number of LacNAc repeating units on *N*-glycans.

120 The glycans on the cell surface were first characterized using flow cytometry with

121 standard lectins. An alive, single-cell population was selected using a standard gating

122 strategy, and mean fluorescence intensities were calculated over the cell population

123 (Fig. 2).

124 *Sambucus nigra* agglutinin (SNA) [33] was used to detect α2,6-linked SIAs, which are

125 present in higher quantities on hCK cells than MDCK cells due to the overexpression

126 of ST6GAL1. The B3GNT2 and/or B4GALT1 knock-ins did not cause substantial

127 differences in α2,6-linked SIA display, which is understandable since we did not

6

128   interfere with the sialyltransferases. *Lycopersicon esculentum* lectin (LEL) recognizes

129   elongated glycans [34] and we observed that glycans capped with α2,6-linked SIAs

130   need at least four consecutive LacNAc repeating units to be recognized, while glycans

131   capped with α2,3-linked SIAs are recognized when presented on two successive

132   LacNAc repeating units (Fig. S1), which explains the lower signal for all hCK cells in

133   general. A substantial increase in the binding of LEL to MDCK-B4GALT1 and MDCK-

134   B3GNT2-B4GALT1 compared to WT MDCK cells was observed, indicating that the

135   LacNAc repeating units on MDCK cells are indeed elongated by the overexpression

136   of mainly B4GALT1. Moreover, we observed an increase in LEL signal in the hCK-

137   B3GNT2 cells compared to the hCK WT cells, indicating that the overexpression of

138   B3GNT2 resulted in the formation of longer glycans on hCK cells. *Erythrina cristagalli*

139   lectin (ECA) recognizes terminal galactose, and thus glycans lacking SIA capping [35].

140   The results using ECA indicated that all MDCK cells have a larger proportion of non-

141   sialylated glycans compared to all hCK cells, which agrees with the overexpression of

142   ST6GAL1 in all hCK cells. No major differences in the amount of non-sialylated

143   glycans between WT and B3GNT2 and/or B4GALT1 knock-in cells were observed.

144   In addition to commonly employed plant lectins, viral proteins were used to examine

145   the glycans displayed on the cells. The N-terminal domain of γCoV/AvCoV/guinea

146   fowl/France/14032/2014 (Gf-CoV-2014 NTD) is known to bind elongated glycans [36].

147   MDCK-B4GALT1 and MDCK-B3GNT2-B4GALT1 cells showed an increased Gf-CoV-

148   2014 NTD signal compared to MDCK WT cells. Furthermore, hCK WT cells appeared

149   to have a higher number of LacNAc repeating units on glycans than MDCK WT cells.

150   The hCK-B3GNT2 cells, and the hCK-B4GALT1 and hCK-B3GNT2-B4GALT1 cells to

151   a lesser extent, showed a substantial increase in Gf-CoV-2014 NTD binding compared

152   to the hCK WT cells, indicating the presence of additional LacNAc repeating units on

7

153   glycans. The HA of A/Vietnam/1203/2004 H5 (H5VN) is commonly used to probe the

154   presence of α2,3-linked SIAs [35, 37, 38]. We observed a much lower amount of α2,3-

155   linked SIAs in all hCK cells compared to all MDCK cells, which is in agreement with

156   the knock-outs of all β-galactoside α-2,3 sialyltransferases that were made in the hCK

157   cells previously [15]. The B3GNT2/B4GALT1 knock-ins did not alter the α2,3-linked

158   SIA content. The HA of the human IAV A/Puerto-Rico/8/1934 (PR8) H1 binds α2,6-

159   linked SIAs [39] and showed increased binding to all hCK cells compared to all MDCK

160   cells, which is related to the overexpression of ST6GAL1 in hCK cells [15]. Increased

161   binding of PR8 to MDCK-B4GALT1 and MDCK-B3GNT2-B4GALT1 compared to

162   MDCK WT cells was also observed, which deviates from the results obtained with

163   SNA, with which no increase in α2,6-linked SIAs was shown.

164   **hCK-B3GNT2 cells are preferentially bound by contemporary H3 HAs**

165   After initial characterization, an array of human H3 HAs was used for flow cytometric

166   binding studies with B3GNT2 and B4GALT1 knock-in cells (Fig. 2C). To cover a broad

167   scope of receptor binding specificities, HAs from viruses from different years (1968-

168   2019) and (sub)clades were chosen. Three HAs from the 3C.2a subclade

169   (A/Singapore/INFH-16-0019/2016,   A/Netherlands/00010/2019,   and   A/Hong-

170   Kong/4801/2014) were chosen to assess the presence of glycans with elongated

171   LacNAc structures [12] on the MDCK and hCK WT and B3GNT2/B4GALT1 knock-in

172   cells.

173   These human H3 HAs prefer binding to α2,6-linked SIAs over α2,3-linked SIAs and

174   therefore, in general, more binding is observed to hCK WT cells than to MDCK WT

175   cells. The HA of A/Hong-Kong/1/1968 does not require multiple consecutive LacNAc

176   repeating units for binding, but it does show a strong preference for glycans with three

177   or four consecutive LacNAc repeating units compared to glycans with only one or two

8

178   repeating units [8]. The preference of A/Hong-Kong/1/1968 for longer glycans is

179   however not observed in our flow cytometry experiments, since the B3GNT2 and

180   B4GALT1 knock-in cells did not show increased binding.

181   The human H3N2 IAVs A/Netherlands/109/2003 and A/Netherlands/761/2009 were

182   previously shown to bind glycans with both two and three, but not one, consecutive

183   LacNAc repeating units [12]. Increased binding of A/Netherlands/109/2003 to MDCK-

184   B4GALT1, MDCK-B3GNT2-B4GALT1, and all hCK cells compared to MDCK WT cells

185   was observed. Interestingly, the MDCK-B4GALT1 and MDCK-B3GNT2-B4GALT1

186   cells often showed comparable or higher binding to the recent H3 HAs than the hCK

187   WT cells, while low levels of α2,6-linked SIAs are present on all MDCK cells. Similar

188   binding patterns were observed for A/Netherlands/761/2009, although the binding to

189   hCK-B3GNT2 cells was much more pronounced.

190   Contemporary H3 IAVs are known to bind to glycans with multiple consecutive LacNAc

191   repeating units [2, 4-12]. This binding specificity is most pronounced for H3N2 viruses

192   of subclade 3C.2a, which require at least three subsequent LacNAc repeating units

193   for binding [12]. Increased binding to MDCK-B4GALT1, MDCK-B3GNT2-B4GALT1,

194   and all hCK cell lines compared to MDCK WT cells was observed for the recent H3

195   HAs (2014-2019) A/Netherlands/354/2016, A/Singapore/INFH-16-0019/2016

196   (subclade 3C.2a), A/Kansas/14/2017 (3C.3a), and A/Netherlands/00010/2019

197   (subclade 3C.2a). The hCK-B3GNT2 cells that were already indicated to have the

198   longest glycans by LEL and Gf-CoV-2014 NTD, also showed a substantial increase in

199   binding of these recent H3 HAs compared to all other cell lines investigated. The strong

200   binding to hCK-B3GNT2 cells of A/Hong-Kong/4801/2014 (subclade 3C.2a) was even

201   more obvious, as other cell lines appear to be barely bound to this HA.

Lectin binding to cells is concentration and sialic acid-dependent

202 To investigate whether the binding of the H3 HAs in the flow cytometry experiments

204 was indeed specific for SIAs, we performed experiments with neuraminidase-treated

205 cells (Fig. S2). As controls for the removal of α2,3-linked or α2,6-linked SIAs,

206 A/Vietnam/1203/2004 [35, 37, 38] and SNA [33] were used. These lectins showed a

207 substantial decrease in the binding signal after neuraminidase treatment. When testing

208 two H3 HAs with well-defined binding specificities, A/Netherlands/109/2003 and

209 A/Netherlands/761/2009 [12], similar results were obtained, indicating that the binding

210 of H3 HAs was indeed SIA-dependent

211 When examining the binding of the HAs of human H3N2 viruses to cells in Fig. 2C,

212 there appeared to be no binding to the MDCK WT cells at all for A/Hong-Kong/1/1968,

213 A/Netherlands/761/2009, A/Hong-Kong/4801/2014, A/Netherlands/354/2016,

214 A/Singapore/INFH-16-0019/2016, A/Kansas/14/2017, and

215 A/Netherlands/00010/2019, even though it is possible to propagate these viruses in

216 MDCK WT cells. To investigate whether binding to MDCK cells occurred at all, a

217 titration with H3 HAs was performed. As a positive control, A/Netherlands/109/2003

218 was used since binding was observed in Fig. 2C. Furthermore, the HAs of the well-

219 defined A/Hong-Kong/1/1968 [8] and the subclade 3C.2a virus A/Singapore/INFH-16-

220 0019/2016 were used. The titration indicated that there is indeed binding to MDCK WT

221 cells but to a much lesser extent than to hCK WT (or hCK-B3GNT2 cells) (Fig. S3).

222 From the flow cytometric experiments, it appeared that the hCK-B3GNT2 cells present

223 the highest number of LacNAc repeating units compared to the other cell lines

224 investigated.

Elongated glycans are detected on hCK-B3GNT2 and hCK-B4GALT1 cells

Since *N*-glycans are the most relevant receptors on cells for IAV [40], we further investigated the *N*-glycans of WT and B3GNT2/B4GALT1 knock-in MDCK and hCK by mass spectrometry of released *N*-glycans. Compared to MDCK WT cells, all seven other cell lines showed a large reduction in the relative abundance of high-mannose glycans (Fig. S4A), to which IAV does not bind. This increase in the relative abundance of complex and hybrid *N*-glycans may partially explain the improved binding phenotype of the H3 HAs to cell lines different than MDCK WT as observed in the flow cytometry experiments (Fig. 2C).

From the flow cytometry experiments, the hCK-B3GNT2 cells were expected to have the highest number of LacNAc repeating units compared to the other seven cell lines (Fig. 2C). The data obtained from the glycan mass spectrometry experiments indeed showed a higher relative abundance of elongated glycans with more than four LacNAc repeating units in hCK-B3GNT2 compared to hCK WT cells (Fig. 3A). Since we were unable to determine the exact structure of the glycans, glycans with at least four LacNAc repeating units were considered as potential receptors for contemporary H3N2 IAVs, since one of the LacNAc repeating units is often present on the other arm [12] and three consecutive LacNAc repeating units are required.

The *N*-glycans with at least one LacNAc repeating unit were further analyzed to determine the relative abundance of glycans with a different number of LacNAc repeating units in the eight different cell lines (Fig. 3B). Knock-in cell lines MDCK-B4GALT1 and MDCK-B3GNT2-B4GALT1 did not show an increase in the number of LacNAc repeating units compared to MDCK WT cells. In MDCK-B3GNT2 and hCK WT cells, the relative increase of glycans with four LacNAc repeating units was a few percent compared to MDCK WT cells. The relative abundance of elongated glycans

11

250 was even higher in hCK-B3GNT2-B4GALT1 cells. Surprisingly, hCK-B4GALT1

251 showed a substantial increase in the relative abundance of glycans with a higher

252 number of LacNAc repeating units, up to even nine LacNAcs (Table S7), which was

253 not expected from the results of the flow cytometry experiments. The highest increase

254 in the relative abundance of elongated glycans was observed in hCK-B3GNT2 cells,

255 which agrees with the flow cytometric results.

256 For binding of contemporary H3N2 IAVs, *N*-glycans with at least three consecutive

257 LacNAc repeating units should also be capped with α2,6-linked SIAs. While we were

258 unable to determine the SIA linkage, we analyzed the percentage of sialylation of the

259 glycans with at least one LacNAc repeating unit (Fig. S4B). In general, 75-96% of

260 these *N*-glycans were sialylated, except for the glycans of MDCK-B3GNT2 cells (38%

261 sialylated), which correlated with the low binding of H3 HAs as observed using flow

262 cytometry (Fig. 2C). Whereas non-sialylated glycans occurred in all groups of LacNAc

263 lengths in MDCK WT and B3GNT2/B4GALT1 knock-in cells, all glycans with at least

264 four LacNAc repeating units (except for 4 glycans in total) on all hCK cell lines were

265 sialylated (Table S1-8).

266 **Sugar nucleotides are not a limiting factor in the biosynthesis of poly-LacNAc**

267 **structures**

268 Changes in sugar nucleotide levels have been observed in cells after overexpression

269 of B3GNT2 and B4GALT1 [31], which may be a limiting factor in the elongation of

270 glycans. Therefore, the concentrations of sugar nucleotides in the cell lysates of

271 MDCK WT, hCK WT, and hCK-B3GNT2 cells were measured by mass spectrometry

272 (Fig. 4, with details in Fig. S5) [41]. The overexpression of ST6GAL1 in hCK WT and

273 hCK-B3GNT2 cells compared to MDCK WT cells resulted in elevated levels of

274 sialylation and thereby lower levels of available CMP-Neu5Ac, which was also

275 demonstrated in the sugar nucleotide analysis. No other major differences or

276 depletions of sugar nucleotides were observed in any of the cell lines. Most

277 importantly, the sugar nucleotides that are required for the biosynthesis of LacNAc

278 repeating units (UDP-galactose and UDP-HexNAc) were not depleted in any of the

279 cell lines, thus sugar nucleotide availability is likely not a limiting factor for the

280 elongation of glycans.

281 **Improved binding of hemagglutinins to cells does ensure higher virus titers**

282 MDCK WT, hCK WT, and B3GNT2 and/or B4GALT1 knock-in cells were inoculated

283 with H3N2 viruses to investigate whether higher titers could be obtained in the knock-

284 in cells. Four control viruses (H3N2 from 2003, H1N1, and influenza B, Fig. 5A) and

285 eight recent (2017-2019) H3N2 viruses from the 3C.2a (Fig. 5B) and 3C.3a (Fig. 5C)

286 subclades were used for inoculation. For the H3N2 virus from 2003, the H1N1 virus,

287 and the influenza B viruses, no substantial difference was observed between the virus

288 titers obtained in MDCK, hCK, or B3GNT2/B4GALT1 knock-in cells (Fig. 5A).

289 Recent 3C.2a viruses are known to only bind glycans having at least three consecutive

290 LacNAc repeating units, while recent 3C.3a viruses also bind glycans with two

291 consecutive LacNAc repeating units [12]. For the 3C.2a viruses, a considerable

292 difference was visible between the titers in MDCK WT and hCK WT cells (Fig. 5B),

293 which correlates with the increased binding as observed in the flow cytometric

294 experiments (Fig. 2). Surprisingly, no substantial difference between the titers in hCK

295 WT and hCK-B3GNT2 cells was observed, while the glycans on the latter cell line were

296 extended as observed in the flow cytometry (Fig. 2) and glycan mass spectrometry

297 experiments (Fig. 3). Furthermore, no difference was observed in the titers for the

298 3C.3a viruses (Fig. 5C), not even between MDCK and hCK cells. Therefore, we

13

299   concluded that additional binding does not necessarily lead to a higher infection

300   efficiency.

301   Isolation of influenza viruses in hCK-B3GNT2 cells is not improved as compared

302   to hCK WT cells

303   While additional H3N2 viruses can be isolated in hCK cells as compared to MDCK-

304   SIAT1 and MDCK cells [15], we noticed that some H3N2 viruses could still not be

305   isolated in hCK cells. To investigate whether cell lines with longer glycans (hCK-

306   B3GNT2 cells) would facilitate the isolation of additional viruses, we attempted to

307   isolate twelve H3N2 viruses (clade 3C.2a) from original patient material in hCK and

308   hCK-B3GNT2 cells (Fig. 5D). Eight of those viruses could not be isolated previously

309   since they did not replicate in hCK cells. All viruses that were previously isolated in

310   hCK cells were again successfully isolated. However, the use of hCK-B3GNT2 cells

311   did not result in more efficient isolation of those viruses. One of the viruses that was

312   not isolated previously (A/Netherlands/173/2019) could now be isolated in both hCK

313   and hCK-B3GNT2 cells. None of the other viruses that could not be isolated previously

314   could now be isolated in either hCK or hCK-B3GNT2. Therefore, a higher number of

315   extended glycans did not improve the isolation of H3N2 IAVs from the 3C.2a clade.

14

Discussion

Although we elongated the LacNAc repeating units on the glycans of MDCK and hCK cells, it did not result in a higher infection efficiency of recent H3N2 IAVs. It has been reported that a low but critical threshold of high-affinity receptors is required for infection [29, 30], though binding and infection are further assisted by the presence of high-abundance low-affinity receptors [28]. This implies that increased HA binding will lead to enhanced entry efficiency. It is therefore counterintuitive that presenting preferred ligands in copious amounts does not lead to increased infection. Strikingly, here we demonstrated that increased HA binding to cells does not necessarily result in more efficient infection.

On the other hand, several studies have indicated that increasing the number of preferred receptors will increase the infection efficiency of IAVs [15, 21, 22, 27], which was also shown with MDCK-SIAT1 [21], MDCK-AX4 [22], and hCK [15] cells. A possible explanation for this discrepancy may lie in the glycoproteins on which *N*-glycans, the presumed glycan receptors for IAVs [40], are presented. It has been suggested previously that only specific sialylated glycoproteins can be used as a receptor for IAV [40, 42], such as the voltage-dependent Ca^{2+} channel $Ca_v1.2$ [43], NKp44 [44, 45], NKp46 [45-47], epidermal growth factor (EGFR) [48], and nucleolin [49]. Although we demonstrated that glycans on B3GNT2/B4GALT1 knock-in cells contained a higher number of LacNAc repeating units, we have not determined on which glycoproteins the elongated glycans are present. Possibly, the glycans that are used as a receptor and are present on specific glycoproteins can be modified in their SIA linkage, as done in MDCK-SIAT1, MDCK-AX4, and hCK cells, but not in the number of LacNAc repeating units. This would explain why the infection efficiency

15

340   could not be increased by the elongation of LacNAc repeating units on MDCK and

341   hCK cells.

342   Nevertheless, not all recent H3N2 IAVs could be isolated efficiently in hCK cells [15],

343   as also shown in Fig. 5D. Possibly, no viable virus particles were present in the patient

344   samples from which we attempted to isolate virus. Alternatively, we may be

345   overlooking an identified [43-49] or an unidentified glycoprotein that is not present (in

346   high enough quantities) on hCK cells. Additionally, our *N*-glycan analysis did not allow

347   for exact glycan structure determination, and therefore it is unclear how many

348   consecutive LacNAc repeating units are present on the glycans. Furthermore, other

349   types of glycans, such as phosphorylated [50] and sulfated glycans [2, 10, 51],

350   possibly act as a receptor for IAV. Due to our sample preparation for the released

351   glycan mass spectrometry analysis, we were unable to measure phosphorylated and

352   sulfated glycans. To increase the isolation of recent H3N2 IAVs, it is of foremost

353   importance to investigate the limiting factor in the infection efficiency of these viruses.

354   The overexpression of B3GNT2 and/or B4GALT1 is responsible for the elongation of

355   glycans. Previously, overexpression of B4GALT1 was found to result in the elongation

356   of glycans on CHO cells [31]. From the flow cytometry analysis, B4GALT1 appeared

357   to be the limiting factor for the elongation of glycans in MDCK cells, while the

358   elongation was limited by B3GNT2 in hCK cells. The glycan mass spectrometry results

359   showed that the relative abundance of glycans with high numbers of LacNAc repeating

360   units was only marginally increased by the overexpression of either or both B3GNT2

361   and B4GALT1, while the glycans on hCK cells were elongated by the overexpression

362   of either B3GNT2 or B4GALT1. The glycans that are investigated in both methods are

363   different since we look at all glycans (*N*-glycans, *O*-glycans, and glycolipids) in flow

364   cytometry experiments and only *N*-glycans during glycan mass spectrometry. In both

16

365   methods, the hCK-B3GNT2 were shown to have the highest relative abundance of

366   elongated LacNAc repeating units. In hCK cells, sialyltransferase expression is

367   severely modified by the overexpression of ST6GAL1 and the knockout of all ST3GAL

368   enzymes. Both the heavily overexpressed ST6GAL1 and B3GNT2 in hCK cells use

369   galactose as a substrate. The overexpression of B3GNT2 in hCK cells perhaps

370   restores the balance between ST6GAL1 and B3GNT2, thereby allowing B3GNT2 to

371   use the galactose as a substrate again for the elongation of glycans before sialylation

372   takes place. On the other hand, in MDCK cells, the balance may be skewed even more

373   by the overexpression of B3GNT2, leading to the low sialylation of glycans on these

374   cells (Fig. S4B).

375   Our observations indicate that only few suitable glycan receptors are required for

376   efficient infection. This is in line with our previous observations that a slight increase

377   from 2.7% to 8.7% of sialylated glycans with at least three consecutive LacNAc

378   repeating units on turkey erythrocytes allowed for the binding of contemporary H3N2

379   viruses [12]. Also in ferrets, an animal model that is often used to study human

380   influenza viruses [38], the presence of glycans in the respiratory tract (lung, trachea,

381   soft palate, nasal turbinate, nasal wash) was investigated. Elongated glycans were

382   present solely as *N*-glycans, with a maximum of 9 LacNAc repeating units per glycan,

383   but at most 0.17% of the detected glycans had at least three consecutive LacNAc

384   repeating units terminating with SIA, which is required for H3N2 IAV binding [52].

385   Although the glycans in the human trachea have not been analyzed yet, data is

386   available on other parts of the human airway system. Sensitive methods indicated the

387   presence of extended *N*-glycans with up to 10 LacNAc repeating units in human lung

388   tissue. However, at most 0.3% of the *N*-glycans were found to contain at least 3

389   consecutive LacNAc repeating units. The *N*-glycans in the bronchus and nasopharynx

17

390   contained a lower number of LacNAc repeating units than in the lung [53]. Another

391   study found *N*-glycans with up to 22 LacNAc repeating units in the lung. Even though

392   the majority of the SIAs were found to be α2,6-linked instead of α2,3-linked, the α2,6-

393   linked SIAs were mainly present on the shorter glycans [54], further supporting that

394   only minor amounts of suitable glycan receptors are required for efficient infection.

Material and Methods

Cell culturing and preparation of cell lysates

Cells were cultured in DMEM (Gibco) with 10% FCS (S7524, Sigma) and 1% penicillin and streptomycin (Sigma). All hCK cells [15], knock-in and WT, were maintained with an additional 10 µg/ml blasticidin and 2 µg/ml puromycin in the medium. B3GNT2 and B4GALT1 knock-in cells were maintained in medium containing an additional 300 µg/ml Hygromycin B, a concentration that was determined to kill MDCK and hCK without Hygromycin B resistance genes. Detaching of the (knock-in) MDCK and hCK cells was always done using TrypLE Express Enzyme (12605010, Thermo Fisher Scientific).

Cell lysates were obtained after first washing cell monolayers once using D-PBS (D5837, Sigma). Cells were subsequently harvested after incubation at 37°C for 20 min with TrypLE Express Enzyme. The cell suspension was centrifuged for 5 min at 250 rcf. The cell pellets were lysed by the addition of RIPA lysis buffer (20-188, Merck Millipore) supplemented with protease inhibitor (A32965, Thermo Fisher Scientific), which was vortexed for 20 sec. The suspension was incubated on ice for 30 min, after which it was centrifuged at 16500 rcf in a fixed-angle centrifuge at 4°C, after which the supernatant was used as cell lysate.

Cloning of lentiviral transfer plasmids

Plasmid pCF525-EF1a-Hygro-P2A-mCherry-lenti [55] was a gift from Jennifer Doudna (Addgene plasmid # 115796) and was used as the backbone for the transfer plasmid. Three transfer plasmids were constructed (pCF-B3GNT2, pCF-B4GALT1, and pCF-B3GNT2-B4GALT1). The region between the P2A and WPRE was removed and replaced by either the *B3GNT2* or *B4GALT1*. When the genes of both

19

419   glycosyltransferases were cloned into the plasmid they were connected with a T2A

420   self-cleaving peptide. The *B3GNT2* and *B4GALT1* genes were always proceeded by

421   the signal sequence of the human GalT, which we copied from the EGFP-GalT

422   plasmid (gift from Jennifer Lippincott-Schwartz, Addgene plasmid # 11929) [56]. The

423   T2A self-cleaving peptide was amplified from plasmid tetO.Sox9.Puro [57], which was

424   a gift from Henrik Ahlenius (Addgene plasmid # 117269). The *B3GNT2* and *B4GALT1*

425   genes were amplified from plasmids B3GNT2-pGEn2-DES and B4GALT1-pGEn2-

426   DES, which are a gift from Kelly Moremen and are available via

427   http://glycoenzymes.ccrc.uga.edu/. All segments were amplified with an overhang,

428   using the primers indicated in Table 1. Assembly of the plasmids was performed using

429   Gibson assembly, after which they were sequenced to ensure correct amplification

430   and assembly.

431   **Table 1. Primers used for the generation of the transfer plasmids.** In brackets is

432   indicated which segment is amplified, and the other part of the name indicates the

433   overhang. The overhang is marked in bold in the sequence.

Primer	Sequence	Used in plasmid
B4GALT1-(pCF)-fwd	**GGACACCGAGCT**ACGCGTTAAGTCGACAATC	pCF-B3GNT2-B4GALT1 pCF-B4GALT1
ss-(pCF)-rev	**CCGAAGCCTCAT**CGGTCCAGGATTCTCTTC	pCF-B3GNT2-B4GALT1 pCF-B3GNT2 pCF-B4GALT1
pCF-(ss)-fwd	**GAATCCTGGACCG**ATGAGGCTTCGGGAGCCG	pCF-B3GNT2-B4GALT1 pCF-B3GNT2 pCF-B4GALT1
B3GNT2-(ss)-rev	**CTTTTCCATTTTT**CTGCAGCGGTGTGGAGAC	pCF-B3GNT2-B4GALT1 pCF-B3GNT2
ss-(B3GNT2)-fwd	**ACACCGCTGCAG**AAAAATGGAAAAGGGGAAG	pCF-B3GNT2-B4GALT1 pCF-B3GNT2
T2A-(B3GNT2)-rev	**CCCCTGCCCTCTCTAGAGGG**GCATTTTAAATGAGCACTCTGCAAC	pCF-B3GNT2-B4GALT1
B3GNT2-(T2A)-fwd	**GTTGCAGAGTGCTCATTTAAAATGC**CCCTCTAGAGAGGGCAGGGGAAG	pCF-B3GNT2-B4GALT1
ss-(T2A)-rev	**CTCAGGAGCGGCTCCCGAAGCCTCAT**CTCGAGTGGGCCGGGATTTTCC	pCF-B3GNT2-B4GALT1
T2A-(ss)-fwd	**GGAAAATCCCGGCCCACTCGAGATGAG**GCTTCGGGAGCCGCTCCTGAG	pCF-B3GNT2-B4GALT1
B4GALT1-(ss)-rev	**CACTGTTCGAGCC**CTGCAGCGGTGTGGAGAC	pCF-B3GNT2-B4GALT1 pCF-B4GALT1
ss-(B4GALT1)-fwd	**GGTCGGAGTCTCCACACCGCTGCAG**GGCTCGAACAGTGCCGCCGCCATC	pCF-B3GNT2-B4GALT1 pCF-B4GALT1

20

pCF-(B4GALT1)-rev	**GAGGTTGATTGTCGACTTAACGCGT**AGCTCGGTGTCCCGATGTCCACTG	pCF-B3GNT2-B4GALT1 pCF-B4GALT1
B3GNT2-(pCF)-fwd	**TTTAAAATGC**ACGCGTTAAGTCGACAATC	pCF-B3GNT2
pCF-(B3GNT2)-rev	**CTTAACGCGT**GCATTTTAAATGAGCACTC	pCF-B3GNT2

434

Lentiviral integration of the *B3GNT2* and *B4GALT1* genes

436 Lentiviral particles were produced using HEK293T cells [58]. One of the transfer

437 plasmids as described above, together with the packaging plasmids pMDLg/pRRE,

438 pRSV-Rev, and pMD2.G were used, which were kind gifts from Didier Trono [59]

439 (Addgene plasmids #12251, #12253, and #12259 respectively). The day before

440 transduction, MDCK and hCK cells were seeded in a 6 wells plate at a density of

441 100.000 cells per well. Transduction with 0.5-3 μl of lentivirus was performed in

442 presence of 8 μg/ml polybrene with 1 ml fresh medium per well. The medium was

443 replaced with fresh medium containing 300 μg/ml Hygromycin B at 18 hours after

444 transduction. Cells were grown until no Hygromycin B sensitive cells were remaining.

445 Cells were always maintained in the presence of 300 μg/ml Hygromycin B.

RT-qPCR analysis on *B3GNT2*, *B4GALT1*, and *ST6GAL1* genes

447 RNA extraction was performed using the GeneJET RNA purification kit (Thermo Fisher

448 Scientific) according to the manufacturer's protocol, after which the DNA was treated

449 with DNAse I (#EN0251, Thermo Fisher Scientific). RT-qPCR was performed using

450 the Luna universal one-step RT-qPCR kit (#E3005, New England Biolabs) according

451 to the provided protocol, in which 10 ng of DNAse I-treated RNA was used. Primers

452 (Table 2) for *B3GNT2*, *B4GALT1*, and *ST6GAL1* were designed to anneal both in the

453 human and dog genome. Primers for GAPDH (household/reference gene) were

454 designed using the dog genome. Experiments were performed in triplicate and Ct

455 values of the RT-qPCR experiments on the glycosyltransferases were compared to

456 the average Ct value of GAPDH of that specific cell line under the assumption that the

21

457   amount of DNA doubles every cycle. The means and standard deviations of the

458   amount of DNA relative to GAPDH were calculated.

459   **Table 2. Primers used in the RT-qPCR experiments**

Primer	Sequence
B4GALT1-fw	GACGTGGACCTCATTCCAA
B4GALT1-rev	CCCAATAATTATTAGGAAATCCATTGAT
B3GNT2-fw	GACGTTTATACTGGAATGTGCC
B3GNT2-rev	CATCTCTTGAGGTTTTCTACTATG
ST6GAL1-fw	GATCATGACGCAGTCCTGAG
ST6GAL1-rev	GGTCCCATACAATTAGGATTCC
GAPDH-fw	GTCGGAGTGAACGGATTTG
GAPDH-rev	GGAATTTGCCGTGGGTAG

460

461   **Overexpression of B3GNT2, B4GALT1, and ST6GAL1 on the protein level**

462   Cell lysates, obtained as described above, were further used for the label-free

463   quantification of B3GNT2, B4GALT1, and ST6GAL1 proteins. From the cell lysates,

464   10 µg of protein was denatured, reduced, and alkylated by adding 100 µl of 150 mM

465   Tris, 5mM TCEP (tris(2-carboxyethyl)phosphine), 30 mM chloroacetamide (CAA), 1%

466   sodium deoxycholate (SDC) at pH 8.5. Next, 100 ng endoproteinase lysC and 100 ng

467   trypsin were added and the samples were incubated overnight at 37°C. The samples

468   were then acidified by adding formic acid (FA) to a concentration of 0.5% before solid-

469   phase extraction (SPE) sample clean-up, causing the SDC to precipitate. SPE clean-

470   up was performed on an Oasis HBL u-elution plate.

471   After the SPE clean-up, the samples were dried with a vacuum centrifuge.

472   Subsequently, the sample was reconstituted in 2% FA before analysis on the Orbitrap

473   Exploris mass spectrometer (Thermo Scientific) connected to a UHPLC 3000 system

474   (Thermo). Approximately 200 ng of reconstituted peptides were trapped on a pre-

475   column and then separated on a 50 cm x 75 µm Poroshell EC-C18 analytical column

22

476   (2.7 µm) temperature controlled at 40°C. Solvent A consisted of 0.1% FA, solvent B of

477   0.1% FA in 80% acetonitrile, and different combinations of solvent A and B were used

478   in the next steps. Trapping was performed for 2 min in 9% solvent B. Peptides were

479   separated by a 65 min gradient of 9–44 % buffer B followed by 44–99% B in 3 min,

480   and 99% B for 4 min. Mass spectrometry (MS) data were obtained in a data-dependent

481   acquisition mode. The full scans were acquired in the m/z range of 350-1600 at the

482   resolution of 60,000 (m/z 400) with AGC target 3E6. The most intense precursor ions

483   were automatically selected for HCD fragmentation performed at normalized collision

484   energy 28, after accumulation to the target value of 1E5. MS/MS acquisition was

485   performed at a resolution of 15,000. Protein identification was done with Byonic

486   (Protein Metrics). A search was performed against the dog proteome

487   (UP000002254_9615) with the addition of the human B3GNT2, B4GALT1, and

488   ST6GAL1 sequences. The search was performed with specific digestion C-terminal of

489   R/K, allowing 3 missed cleavages, using precursor and fragment mass tolerances of

490   12 and 24 ppm, respectively. Carbamidomethylation of cysteine was set as a fixed

491   modification and oxidation of the methionine or tryptophan as a variable modification.

492   Peptides unique for the human B3GNT2, B4GALT1, and ST6GAL1 were manually

493   selected and the MS1 peak areas were integrated with Skyline and normalized against

494   the combined MS1 signals for identified peptides of tubulin beta (E2RFJ7). The

495   peptide library for Skyline was built by repeating the search with a focused database

496   containing only the human B3GNT2, B4GALT1, and ST6GAL1 and tubulin beta

497   sequences. The mass spectrometry proteomic data have been deposited to the

498   ProteomeXchange Consortium via the PRIDE [60] partner repository with the dataset

499   identifier PXD037175.

Expression and purification of trimeric HA for binding studies

500 Recombinant trimeric IAV hemagglutinin proteins (HA) were cloned into the pCD5

501 expression vector as described previously [61, 62], in frame with a GCN4 trimerization

502 motif (KQIEDKIEEIESKQKKIENEIARIKK), a superfolder GFP [39] or mOrange2 [63]

503 and the Twin-Strep-tag (WSHPQFEKGGGSGGGSWSHPQFEK); IBA, Germany). The

504 open reading frames of the HAs of A/Vietnam/1203/2004 H5 (Addgene plasmid

505 #182546, [35]), A/Puerto-Rico/8/1934 H1 [39], A/Hong-Kong/480/2014 H3 (3C.2a),

506 A/Netherlands/109/2003 H3, A/Netherlands/761/2009 H3, A/Netherlands/354/2016

507 H3, A/Netherlands/00010/2019 H3 (3C.2a), A/Hong-Kong/1/1968 H3,

508 A/Singapore/INFH-16-0019/2016 H3 (3C.2a), A/Kansas/14/2017 H3 (3C.3a), and the

509 NTD of γCoV/AvCoV/guinea fowl/France/14032/2014 were synthesized and codon-

510 optimized by GenScript. The trimeric HAs were expressed in HEK293S GnTI(-) cells

511 with polyethyleneimine I (PEI) in a 1:8 ratio (μg DNA:μg PEI) for the HAs as previously

512 described [61], while a 1:12 ratio was used for the NTD of the guinea fowl CoV. The

513 transfection mix was replaced after 6 hours by 293 SFM II suspension medium

514 (Invitrogen, 11686029), supplemented with sodium bicarbonate (3.7 g/L), Primatone

515 RL-UF (3.0 g/L, Kerry, NY, USA), glucose (2.0 g/L), glutaMAX (1%, Gibco), valproic

516 acid (0.4 g/L) and DMSO (1.5%). Culture supernatants were harvested 5 days post-

517 transfection and purified with sepharose strep-tactin beads (IBA Life Sciences,

518 Germany) according to the manufacturer's instructions.

Flow cytometry studies

520 Cells were harvested using TrypLE Express Enzyme as described above. After

521 removal of the supernatant, cells were resuspended in PBS supplemented with 1%

522 FCS (S7524, Sigma) and 2mM EDTA and kept at 4°C at any time. For experiments

523 with α2-3,6,8,9 neuraminidase A (#P0722, New England Biolabs), neuraminidase

24

525 (NA) was used 1:200 with 1,000,000 cells per ml in glycobuffer 1 (5 mM $CaCl_2$, 50 mM

526 sodium acetate, in MQ water, at pH 5.5) for 16 hours at 37°C on a shaking platform in

527 the dark, before incubation with the lectin/HA mixes. In a round-bottom 96-wells plate

528 (353910, Falcon), 150,000 cells were used. Per well, 100 µl of PBS supplemented with

529 1 µg of HA or biotinylated lectin (SNA (B1305), LEL (B1175), ECA (B1145), all from

530 Vector Laboratories) was used, to achieve a final concentration of 10 µg/ml.

531 Hemagglutinins were precomplexed (on ice, 20 min) with 1.3 µg monoclonal antibody

532 detecting the Twin-Strep-tag and 0.325 µg goat anti-human Alexa Fluor 488 (A11013,

533 Invitrogen). Biotinylated lectins were precomplexed (on ice, 20 min) with 0.2 µg

534 streptavidin Alexa Fluor 488 (S32354, Invitrogen). For titration experiments, different

535 amounts of HA, lectin, precomplexing antibodies, or streptavidin were used.

536 Furthermore, eBioscience Fixable Viability Dye eFluor 780 (65-0865, Thermo Fisher

537 Scientific) was diluted 1:2000 in the same mixture. Cells were incubated with the

538 hemagglutinin/lectin mixed for 30 minutes at 4°C in the dark. Cells were washed once

539 with PBS supplemented with 1% FCS and 2 mM EDTA, after which the cells were

540 fixated with 100 µl of 1% paraformaldehyde in PBS for 10 minutes. Afterward, cells

541 were washed once using PBS supplemented with 1% FCS and 2 mM EDTA, after

542 which they were resuspended in 100 µl of the same buffer. Flow cytometry was

543 performed using the BD FACSCanto II (BD Biosciences) using appropriate laser

544 voltages. Data were analyzed using FlowLogic (Inivai Technologies) and gated as

545 described in Fig. 2A to consecutively select cells, single cells, and cells that are not

546 dead. Mean fluorescence values of triplicates were averaged and standard deviations

547 were calculated. Curves for titration experiments were smoothed using the standard

548 settings.

Identification of *N*-glycans on cells by mass spectrometry

Cell lysates of WT and B3GNT2/B4GALT1 knock-in MDCK and hCK cells were obtained as described above. The total protein concentration in the cell lysates was determined using a BCA assay. The glycans in 400 μg of total protein were released by PNGaseF treatment. Proteins were first denatured in DTT/SDS (40 mM DTT, 0.5% v/v SDS) for 8 minutes at 95°C, after which they were cooled on ice. Subsequently, NP-40 (1% v/v) and glycobuffer G7 (50 mM sodium phosphate at pH 7.5) were added, together with 30 μg of PNGaseF. The samples were incubated in a shaking incubator overnight at 37°C. Samples were centrifuged (4700 rcf, 3 min) to remove potential precipitate, after which they were loaded on separate C18 SPE cartridges (Avantor™ 7020-02 BAKERBOND™ SPE Octadecyl), which were beforehand conditioned with 1 ml acetonitrile (MeCN) and 1 ml MQ water. The flow-through was collected and the remaining glycans were eluted from the C18 cartridges with 1 ml of 5% MeCN and 0.05% trifluoroacetic acid (TFA) in MQ water. The MeCN and TFA in both samples were evaporated under a stream of nitrogen gas. Flow through and elution fractions were diluted into 500 μl MQ water and combined, after which PGC SPE cartridges (Thermo Scientific™ HyperSep™ Hypercarb™ SPE cartridges) were used to further purify the samples. The PGC SPE cartridges were conditioned with 1 ml MeCN and 1 ml MQ water, after which the samples were loaded on the cartridges. The cartridges were washed with 1 ml 0.05% TFA in MQ water and 1 ml 5% MeCN with 0.05% TFA in MQ water. Samples were eluted with 50% MeCN and 0.1% TFA in MQ water and evaporated under a stream of nitrogen gas. The dried glycans were dissolved in 30 μl MQ water and 6 μl pure glacial acetic acid and labeled using 5 μl procainamide (105 mg/ml procainamide HCl in DMSO) and 5 μl 2-picoline borane (107 mg/ml 2-Methylpyridine borane complex in DMSO). The solution was vortexed thoroughly and

26

574   incubated for 2 hours at 65°C, after which the samples were evaporated using the

575   vacuum concentrator. The sample was dissolved in 300 µl MQ water and vortexed

576   until the pellets were dissolved, after which 5 µl 25% (w/v) ammonia was added per

577   sample to ensure a pH above 10. To remove the unused procainamide from the

578   reaction mixture, liquid-liquid extraction with 500 µl dichloromethane was performed

579   three times, with centrifuge steps of 4700 rcf for 3 min in between. The

580   dichloromethane was removed and residual dichloromethane was evaporated under

581   a stream of nitrogen gas. The samples were dissolved in a total of 1 ml MQ water after

582   which they were loaded onto PGC SPE cartridges (conditioned with 2 ml MeCN and

583   2 ml MQ water). The cartridges were washed with 2 ml MQ water and the glycans

584   were eluted using 50% MeCN with 0.1% TFA in MQ water, after which the MeCN and

585   TFA were evaporated under a stream of nitrogen gas, followed by lyophilization.

586   Before HILIC-IMS-QTOF analysis, the lyophilized samples were reconstituted in 15 µl

587   70% MeCN in MQ water and centrifuged. The injected volume was 10 µl. The HILIC-

588   IMS-QTOF system was an Agilent 1260 Infinity LC coupled to a 6560 IM-QTOF mass

589   spectrometer (Agilent Technologies, Santa Clara, USA). For HILIC separation, a

590   SeQuant ZIC-cHILIC column (3 µm, 100 Å; 150 x 2.1 mm) was used with a matching

591   guard column (20 x 2.1 mm). The temperature of the column compartment was set at

592   40 ºC. The mobile phase was composed of eluent A: 10 mM ammonium formate with

593   10 mM formic acid in MQ water, and eluent B: LC-MS grade MeCN. The initial eluent

594   composition was 30% A at a flow rate of 0.2 ml/min, followed by a linear gradient to

595   50% A from 0 to 20 minutes. 50% A was held isocratically until 25 minutes. To re-

596   establish initial conditions, the column was flushed with at least 10 column volumes of

597   30% A.

598   The IMS-QTOF was set to positive ion mode with a capillary voltage of 3500 V, nozzle

599   voltage of 2000 V, and a fragmentor voltage of 360 V. The drying gas temperature

600   was 300 ºC with a flow rate of 8 l/min and the sheath gas temperature was 300 ºC at

601   11 l/min. The nebulizer pressure was set at 40 psi. The ion mobility settings were set

602   as follows: 18 IM transients per frame, an IM trap fill time of 3900 µs and a release

603   time of 250 µs, the drift tube voltage was 1400 V, and the multiplexing pulsing

604   sequence length was 4 bits.

605   IM-MS data was calibrated to reference signals of m/z 121.050873 and 922.009798

606   using the IM-MS reprocessor utility of the Agilent Masshunter software. The mass-

607   calibrated data was then demultiplexed using the PNNL preprocessor software using

608   a 5-point moving average smoothing and interpolation of 3 drift bins. To find potential

609   glycan hits in the processed data, the 'find features' (IMFE) option of the Agilent IM-

610   MS browser was used with the following criteria: 'Glycans' isotope model, limited

611   charge state to 5 and an ion intensity above 500. The found features were filtered by

612   m/z range of 300 – 3200 and an abundance of over 500 (a.u.) where abundance for a

613   feature was defined as 'max ion volume' (the peak area of the most abundant ion for

614   that feature).

615   After exporting the list of filtered features, glycans with a mass below 1129 Da (the

616   mass of an *N*-glycan core) were removed. The ExPASy GlycoMod tool [64] was used

617   to search for glycan structures (monoisotopic mass values, 5 ppm mass tolerance,

618   neutral, derivatized N-linked oligosaccharides, procainamide (mass 235.168462302)

619   as reducing terminal derivative, looking for underivatized monosaccharide residues

620   (Hexose, HexNAc, Deoxyhexose, and NeuAc)). For features with multiple potential

621   monosaccharide combinations, the most realistic glycan in the biological context was

622   chosen. The abundance of glycan features with the same mass, composition, and a

623   maximum difference of 0.1 min in the retention time were combined as one isomer.

624   Full glycan composition feature lists for the different cell lines are presented in Table

625   S1-8.

626   Analysis of the number of LacNAc repeating units was performed on the complex and

627   hybrid *N*-glycans with at least one LacNAc repeating unit. A glycan with one LacNAc

628   repeating unit was defined as a glycan with 4 hexoses and a minimum of 3 HexNAcs

629   or 3 HexNAcs and at least 4 hexoses. A glycan with two LacNAc repeating units was

630   defined as a glycan with 5 hexoses and a minimum of 4 HexNAcs or 4 HexNAcs and

631   at least 5 hexoses. This pattern was continued for the higher numbers of LacNAc

632   repeating units. The total absolute abundance of all selected glycans was added up,

633   after which the relative abundance of a given number of LacNAc repeating units was

634   calculated from this total. Additionally, the percentage of these glycans with at least

635   one SIA was calculated.

636   Chromatograms of the *N*-glycans with two to seven LacNAc repeating units, calculated

637   as described above, from hCK WT and hCK-B3GNT2 cells were constructed using

638   Agilent's Masshunter Qualtitative Analysis 10.0 software (Fig. 3A). The shown

639   chromatograms are the summed extracted-ion-count (EIC) for the ten most abundant

640   glycan features per LacNAc repeating unit group. The EIC for a glycan was set as the

641   observed m/z value with a symmetrical 10 ppm expansion. Different ionization states

642   of the same glycan that were found as a separate feature by the feature-finding

643   software were also included in the summed EIC chromatogram.

644   **Sugar nucleotide analysis**

645   Cells were grown to 60-70% confluency in a 6-wells plate, after which the medium was

646   removed and the cells were washed twice with wash buffer (75 mM ammonium

29

647 carbonate in MQ water, pH 7.4 (corrected with glacial acetic acid), at 4°C). The cells

648 were then treated with 700 µl of extraction buffer (40% acetonitrile, 40% methanol,

649 20% MQ water, at 4°C) per well for 2 minutes, after which the supernatant was

650 transferred to a vial. This extraction step is repeated for 3 minutes, after which the two

651 extracts were pooled and centrifuged at 18000 rcf for 3 min. The supernatant was

652 taken and dried in the vacuum concentrator. Samples were frozen at -80°C until

653 analysis using an ion-pair UHPLC-QqQ 1290-6490 Agilent mass spectrometer by

654 Glycomscan BV (Oss, the Netherlands) [41].

655 **Virus titration on B3GNT2/B4GALT1 knock-in MDCK and hCK cells**

656 Virus titers in the virus stocks in Table 3 were determined using end-point titration in

657 MDCK cells and inoculated cell cultures were tested for agglutination activity using

658 turkey red blood cells as an indicator of virus replication in the cells. For recent (2017-

659 2019) H3N2 viruses, no binding to erythrocytes was observed and therefore virus titers

660 were determined using a nucleoprotein (NP) staining. The NP staining was performed

661 on the inoculated cells that were fixed with acetone for at least 20 minutes at -20°C.

662 Primary mouse anti-NP antibody (HB65, 2 mg/ml) was diluted 1:3000 and the

663 secondary goat anti-mouse IgG HRP antibody (A16702, 1 mg/ml, Thermo Fisher

664 Scientific) was used at a dilution of 1:30000, after which 50 µl per well was used for

665 both solutions. True Blue substrate (KPL) was then added to visualize positive wells

666 using an ImmunoSpot Analyzer (CTL Europe, Bonn, Germany). Based on the negative

667 control values and the highest positive values per plate, the cut-off for positivity was

668 determined. Infectious titers were calculated from five replicates using the Spearman-

669 Kärber method [65].

670 **Table 3. Details of IAVs used in the experiment shown in Fig. 5A-C**. These

671 viruses include one older H3N2 virus from 2003, one H1N1 virus, and two influenza

672   B viruses. The viruses were passaged in MDCK, MDCK-SIAT1 [21], and/or hCK

673   cells.

Virus	Clade	Passage history
A/Netherlands/1797/2017	3C.2a1	SIAT2hCK2
A/Netherlands/371/2019	3C.2a1	SIAT2MDCK1hCK1
A/Netherlands/10009/2019	3C.2a1b	SIAT1hCK3
A/Netherlands/314/2019	3C.2a1b	SIAT2hCK2
A/Netherlands/384/2017	3C.3a	SIAT2hCK4
A/Netherlands/10006/2019	3C.3a	SIAT1hCK3
A/Netherlands/3466/2017	3C.2a2	SIAT2hCK2
A/Netherlands/10616/2019	3C.2a2	SIAT1hCK2
A/Netherlands/213/2003	-	MDCK2
A/Netherlands/121/2020	H1N1	hCK2
B/Croatia/7789/2019	Vic	MDCKxMDCK3
B/Netherlands/461/2019	Yam	SIAT5hCK1

674

675   **Inoculation of hCK and hCK-B3GNT2 cells with influenza viruses**

676   To evaluate whether IAVs that could not be isolated previously in hCK cells would

677   replicate in hCK-B3GNT2 cells, hCK and hCK-B3GNT2 cells were seeded at a density

678   of 20.000 cells per well in 96 wells plates at 24 hours before inoculation. The original

679   patient material (100 µl) containing influenza virus (details of viruses in Table 4) was

680   diluted in 700 µl infection medium (EMEM (Cambrex, Heerhugowaard, The

681   Netherlands) supplemented with 100 U/ml penicillin, 100 µg/ml streptomycin, 2mM

682   glutamine, 1.5mg/ml sodium bicarbonate (Cambrex), 10mM Hepes (Cambrex),

683   nonessential amino acids (MP Biomedicals) and 20 µg/ml trypsin (Cambrex)), after

684   which a two-fold dilution series was made. After three days, the cytopathic effects in

685   the cells were evaluated and the mean (n=3) of the number of infected wells was

686   calculated.

687   **Table 4. Details of IAVs used in the experiment shown in Fig. 5D.** The exact

688   virus is indicated as well as the clade and HA mutations if applicable. Previous

31

689   attempts of isolating these viruses in hCK cells were either unsuccessful (-) or

690   successful (+).

Number	Virus	Clade (+ HA mutations)	Cultured previously
1	A/Netherlands/3425/2017	3C.2a	-
2	A/Netherlands/2362/2018	3C.2a1b	-
3	A/Netherlands/2380/2018	3C.2a1b	-
4	A/Netherlands/010/2019	3C.2a1b	-
5	A/Netherlands/173/2019	3C.2a1b	-
6	A/Netherlands/1268/2019	3C.2a4	-
7	A/Netherlands/1735/2019	3C.2a1b + T135K	-
8	A/Netherlands/1747/2019	3C.2a1b + T135K	-
9	A/Netherlands/1439/2019	3C.2a1b	+
10	A/Netherlands/1734/2019	3C.2a1b + T135K	+
11	A/Netherlands/054/2020	3C.2a1b + T131K	+
12	A/Netherlands/008/2021	3C.2a1b.2a2	+

691

32

Acknowledgments

Funding

References

1.   Jester BJ, Uyeki TM, Jernigan DB. Fifty years of influenza A(H3N2) following the pandemic of 1968. Am J Public Health. 2020;110(5):669-76. Epub 2020/04/09. doi: 10.2105/AJPH.2019.305557. PubMed PMID: 32267748; PubMed Central PMCID: PMCPMC7144439.

2.   Stevens J, Blixt O, Glaser L, Taubenberger JK, Palese P, Paulson JC, et al. Glycan microarray analysis of the hemagglutinins from modern and pandemic influenza viruses reveals different receptor specificities. J Mol Biol. 2006;355(5):1143-55. Epub 2005/12/14. doi: 10.1016/j.jmb.2005.11.002. PubMed PMID: 16343533.

3.   Rogers GN, Paulson JC. Receptor determinants of human and animal influenza virus isolates: differences in receptor specificity of the H3 hemagglutinin based on species of origin. Virology. 1983;127(2):361-73. Epub 1983/06/01. doi: 10.1016/0042-6822(83)90150-2. PubMed PMID: 6868370.

4.   Yang H, Carney PJ, Chang JC, Guo Z, Villanueva JM, Stevens J. Structure and receptor binding preferences of recombinant human A(H3N2) virus hemagglutinins. Virology. 2015;477:18-31. Epub 2015/01/27. doi: 10.1016/j.virol.2014.12.024. PubMed PMID: 25617824; PubMed Central PMCID: PMCPMC5696785.

5.   Gulati S, Smith DF, Cummings RD, Couch RB, Griesemer SB, St George K, et al. Human H3N2 influenza viruses isolated from 1968 to 2012 show varying preference for receptor substructures with no apparent consequences for disease or spread. PLoS One. 2013;8(6):e66325. Epub 2013/06/28. doi: 10.1371/journal.pone.0066325. PubMed PMID: 23805213; PubMed Central PMCID: PMCPMC3689742.

6.   Chandrasekaran A, Srinivasan A, Raman R, Viswanathan K, Raguram S, Tumpey TM, et al. Glycan topology determines human adaptation of avian H5N1 virus hemagglutinin. Nat Biotechnol. 2008;26(1):107-13. Epub 2008/01/08. doi: 10.1038/nbt1375. PubMed PMID: 18176555.

7.   Sriwilaijaroen N, Nakakita SI, Kondo S, Yagi H, Kato K, Murata T, et al. N-glycan structures of human alveoli provide insight into influenza A virus infection and pathogenesis. FEBS J. 2018;285(9):1611-34. Epub 2018/03/16. doi: 10.1111/febs.14431. PubMed PMID: 29542865.

8.   Peng W, de Vries RP, Grant OC, Thompson AJ, McBride R, Tsogtbaatar B, et al. Recent H3N2 viruses have evolved specificity for extended, branched human-type receptors, conferring potential for increased avidity. Cell Host Microbe. 2017;21(1):23-34. Epub 2016/12/27. doi: 10.1016/j.chom.2016.11.004. PubMed PMID: 28017661; PubMed Central PMCID: PMCPMC5233592.

9.   Byrd-Leotis L, Gao C, Jia N, Mehta AY, Trost J, Cummings SF, et al. Antigenic pressure on H3N2 influenza virus drift strains imposes constraints on binding to sialylated receptors but not phosphorylated glycans. J Virol. 2019;93(22). Epub 2019/09/06. doi: 10.1128/JVI.01178-19. PubMed PMID: 31484755; PubMed Central PMCID: PMCPMC6819937.

10.   Stevens J, Chen LM, Carney PJ, Garten R, Foust A, Le J, et al. Receptor specificity of influenza A H3N2 viruses isolated in mammalian cells and embryonated chicken eggs. J Virol. 2010;84(16):8287-99. Epub 2010/06/04. doi: 10.1128/JVI.00058-10. PubMed PMID: 20519409; PubMed Central PMCID: PMCPMC2916524.

11.   Nycholat CM, McBride R, Ekiert DC, Xu R, Rangarajan J, Peng W, et al. Recognition of sialylated poly-N-acetyllactosamine chains on N- and O-linked glycans by human and avian influenza A virus hemagglutinins. Angew Chem Int Ed Engl. 2012;51(20):4860-3. Epub 2012/04/17. doi: 10.1002/anie.201200596. PubMed PMID: 22505324; PubMed Central PMCID: PMCPMC3517101.

12.   Broszeit F, van Beek RJ, Unione L, Bestebroer TM, Chapla D, Yang JY, et al. Glycan remodeled erythrocytes facilitate antigenic characterization of recent A/H3N2 influenza viruses. Nat Commun. 2021;12(1):5449. Epub 2021/09/16. doi: 10.1038/s41467-021-25713-1. PubMed PMID: 34521834; PubMed Central PMCID: PMCPMC8440751.

13.   Chambers BS, Li Y, Hodinka RL, Hensley SE. Recent H3N2 influenza virus clinical isolates rapidly acquire hemagglutinin or neuraminidase mutations when propagated for antigenic analyses. J Virol.

755 2014;88(18):10986-9. Epub 2014/07/06. doi: 10.1128/JVI.01077-14. PubMed PMID: 24991002;
756 PubMed Central PMCID: PMCPMC4178893.

757 14. Asaoka N, Tanaka Y, Sakai T, Fujii Y, Ohuchi R, Ohuchi M. Low growth ability of recent influenza
758 clinical isolates in MDCK cells is due to their low receptor binding affinities. Microbes Infect.
759 2006;8(2):511-9. Epub 2005/11/23. doi: 10.1016/j.micinf.2005.08.006. PubMed PMID: 16300986.

760 15. Takada K, Kawakami C, Fan S, Chiba S, Zhong G, Gu C, et al. A humanized MDCK cell line for
761 the efficient isolation and propagation of human influenza viruses. Nat Microbiol. 2019;4(8):1268-73.
762 Epub 2019/05/01. doi: 10.1038/s41564-019-0433-6. PubMed PMID: 31036910.

763 16. Oh DY, Barr IG, Mosse JA, Laurie KL. MDCK-SIAT1 cells show improved isolation rates for recent
764 human influenza viruses compared to conventional MDCK cells. J Clin Microbiol. 2008;46(7):2189-94.
765 Epub 2008/05/16. doi: 10.1128/JCM.00398-08. PubMed PMID: 18480230; PubMed Central PMCID:
766 PMCPMC2446904.

767 17. Lee HK, Tang JW, Kong DH, Loh TP, Chiang DK, Lam TT, et al. Comparison of mutation patterns
768 in full-genome A/H3N2 influenza sequences obtained directly from clinical samples and the same
769 samples after a single MDCK passage. PLoS One. 2013;8(11):e79252. Epub 2013/11/14. doi:
770 10.1371/journal.pone.0079252. PubMed PMID: 24223916; PubMed Central PMCID:
771 PMCPMC3815150.

772 18. Medeiros R, Escriou N, Naffakh N, Manuguerra JC, van der Werf S. Hemagglutinin residues of
773 recent human A(H3N2) influenza viruses that contribute to the inability to agglutinate chicken
774 erythrocytes. Virology. 2001;289(1):74-85. Epub 2001/10/17. doi: 10.1006/viro.2001.1121. PubMed
775 PMID: 11601919.

776 19. Allen JD, Ross TM. H3N2 influenza viruses in humans: Viral mechanisms, evolution, and
777 evaluation. Hum Vaccin Immunother. 2018;14(8):1840-7. Epub 2018/04/12. doi:
778 10.1080/21645515.2018.1462639. PubMed PMID: 29641358; PubMed Central PMCID:
779 PMCPMC6149781.

780 20. Peck H, Laurie KL, Rockman S, Leung V, Lau H, Soppe S, et al. Enhanced isolation of influenza
781 viruses in qualified cells improves the probability of well-matched vaccines. NPJ Vaccines.
782 2021;6(1):149. Epub 2021/12/11. doi: 10.1038/s41541-021-00415-3. PubMed PMID: 34887440;
783 PubMed Central PMCID: PMCPMC8660794.

784 21. Matrosovich M, Matrosovich T, Carr J, Roberts NA, Klenk HD. Overexpression of the alpha-2,6-
785 sialyltransferase in MDCK cells increases influenza virus sensitivity to neuraminidase inhibitors. J Virol.
786 2003;77(15):8418-25. Epub 2003/07/15. doi: 10.1128/jvi.77.15.8418-8425.2003. PubMed PMID:
787 12857911; PubMed Central PMCID: PMCPMC165236.

788 22. Hatakeyama S, Sakai-Tagawa Y, Kiso M, Goto H, Kawakami C, Mitamura K, et al. Enhanced
789 expression of an alpha2,6-linked sialic acid on MDCK cells improves isolation of human influenza
790 viruses and evaluation of their sensitivity to a neuraminidase inhibitor. J Clin Microbiol.
791 2005;43(8):4139-46. Epub 2005/08/06. doi: 10.1128/JCM.43.8.4139-4146.2005. PubMed PMID:
792 16081961; PubMed Central PMCID: PMCPMC1233980.

793 23. Lin Y, Wharton SA, Whittaker L, Dai M, Ermetal B, Lo J, et al. The characteristics and antigenic
794 properties of recently emerged subclade 3C.3a and 3C.2a human influenza A(H3N2) viruses passaged
795 in MDCK cells. Influenza Other Respir Viruses. 2017;11(3):263-74. Epub 2017/02/07. doi:
796 10.1111/irv.12447. PubMed PMID: 28164446; PubMed Central PMCID: PMCPMC5410720.

797 24. Byrd-Leotis L, Jia N, Matsumoto Y, Lu D, Kawaoka Y, Steinhauer DA, et al. Sialylated and
798 sulfated N-Glycans in MDCK and engineered MDCK cells for influenza virus studies. Sci Rep.
799 2022;12(1):12757. Epub 2022/07/27. doi: 10.1038/s41598-022-16605-5. PubMed PMID: 35882911;
800 PubMed Central PMCID: PMCPMC9325728.

801 25. Li T, Liu L, Wei N, Yang JY, Chapla DG, Moremen KW, et al. An automated platform for the
802 enzyme-mediated assembly of complex oligosaccharides. Nat Chem. 2019;11(3):229-36. Epub
803 2019/02/23. doi: 10.1038/s41557-019-0219-8. PubMed PMID: 30792508; PubMed Central PMCID:
804 PMCPMC6399472.

26.   Liu L, Prudden AR, Capicciotti CJ, Bosman GP, Yang JY, Chapla DG, et al. Streamlining the chemoenzymatic synthesis of complex N-glycans by a stop and go strategy. Nat Chem. 2019;11(2):161-9. Epub 2018/12/12. doi: 10.1038/s41557-018-0188-3. PubMed PMID: 30532014; PubMed Central PMCID: PMCPMC6347513.

27.   Lin YP, Xiong X, Wharton SA, Martin SR, Coombs PJ, Vachieri SG, et al. Evolution of the receptor binding properties of the influenza A(H3N2) hemagglutinin. Proc Natl Acad Sci U S A. 2012;109(52):21474-9. Epub 2012/12/14. doi: 10.1073/pnas.1218841110. PubMed PMID: 23236176; PubMed Central PMCID: PMCPMC3535595.

28.   Liu M, Huang LZX, Smits AA, Bull C, Narimatsu Y, van Kuppeveld FJM, et al. Human-type sialic acid receptors contribute to avian influenza A virus binding and entry by hetero-multivalent interactions. Nat Commun. 2022;13(1):4054. Epub 2022/07/14. doi: 10.1038/s41467-022-31840-0. PubMed PMID: 35831293; PubMed Central PMCID: PMCPMC9279479.

29.   Rimmelzwaan GF, Nieuwkoop NJ, de Mutsert G, Boon AC, Kuiken T, Fouchier RA, et al. Attachment of infectious influenza A viruses of various subtypes to live mammalian and avian cells as measured by flow cytometry. Virus Res. 2007;129(2):175-81. Epub 2007/08/24. doi: 10.1016/j.virusres.2007.07.007. PubMed PMID: 17714820.

30.   Kumari K, Gulati S, Smith DF, Gulati U, Cummings RD, Air GM. Receptor binding specificity of recent human H3N2 influenza viruses. Virol J. 2007;4:42. Epub 2007/05/11. doi: 10.1186/1743-422X-4-42. PubMed PMID: 17490484; PubMed Central PMCID: PMCPMC1876801.

31.   Wang Q, Wang T, Yang S, Sha S, Wu WW, Chen Y, et al. Metabolic engineering challenges of extending N-glycan pathways in Chinese hamster ovary cells. Metab Eng. 2020;61:301-14. Epub 2020/07/15. doi: 10.1016/j.ymben.2020.06.007. PubMed PMID: 32663509.

32.   Wang X, Xu Z, Tian Z, Zhang X, Xu D, Li Q, et al. The EF-1alpha promoter maintains high-level transgene expression from episomal vectors in transfected CHO-K1 cells. J Cell Mol Med. 2017;21(11):3044-54. Epub 2017/05/31. doi: 10.1111/jcmm.13216. PubMed PMID: 28557288; PubMed Central PMCID: PMCPMC5661254.

33.   Shibuya N, Goldstein IJ, Broekaert WF, Nsimba-Lubaki M, Peeters B, Peumans WJ. The elderberry (Sambucus nigra L.) bark lectin recognizes the Neu5Ac(alpha 2-6)Gal/GalNAc sequence. J Biol Chem. 1987;262(4):1596-601. Epub 1987/02/05. doi: 10.1016/S0021-9258(19)75677-4. PubMed PMID: 3805045.

34.   Sweeney JG, Liang J, Antonopoulos A, Giovannone N, Kang S, Mondala TS, et al. Loss of GCNT2/I-branched glycans enhances melanoma growth and survival. Nat Commun. 2018;9(1):3368. Epub 2018/08/24. doi: 10.1038/s41467-018-05795-0. PubMed PMID: 30135430; PubMed Central PMCID: PMCPMC6105653.

35.   Broszeit F, Tzarum N, Zhu X, Nemanichvili N, Eggink D, Leenders T, et al. N-glycolylneuraminic acid as a receptor for influenza A viruses. Cell Rep. 2019;27(11):3284-94 e6. Epub 2019/06/13. doi: 10.1016/j.celrep.2019.05.048. PubMed PMID: 31189111; PubMed Central PMCID: PMCPMC6750725.

36.   Bouwman KM, Delpont M, Broszeit F, Berger R, Weerts E, Lucas MN, et al. Guinea fowl coronavirus diversity has phenotypic consequences for glycan and tissue binding. J Virol. 2019;93(10). Epub 2019/03/08. doi: 10.1128/JVI.00067-19. PubMed PMID: 30842318; PubMed Central PMCID: PMCPMC6498037.

37.   Spruit CM, Zhu X, Tomris I, Rios-Carrasco M, Han AX, Broszeit F, et al. N-glycolylneuraminic acid binding of avian and equine H7 influenza A viruses. J Virol. 2022;96(5):e0212021. Epub 2022/01/20. doi: 10.1128/jvi.02120-21. PubMed PMID: 35044215; PubMed Central PMCID: PMCPMC8906439.

38.   Spruit CM, Nemanichvili N, Okamatsu M, Takematsu H, Boons GJ, de Vries RP. N-glycolylneuraminic acid in animal models for human influenza A virus. Viruses. 2021;13(5). Epub 2021/06/03. doi: 10.3390/v13050815. PubMed PMID: 34062844; PubMed Central PMCID: PMCPMC8147317.

39.   Nemanichvili N, Tomris I, Turner HL, McBride R, Grant OC, van der Woude R, et al. Fluorescent trimeric hemagglutinins reveal multivalent receptor binding properties. J Mol Biol. 2019;431(4):842-

856   56. Epub 2019/01/01. doi: 10.1016/j.jmb.2018.12.014. PubMed PMID: 30597163; PubMed Central
857   PMCID: PMCPMC6397626.

858   40.   Chu VC, Whittaker GR. Influenza virus entry and infection require host cell N-linked
859   glycoprotein. Proc Natl Acad Sci U S A. 2004;101(52):18153-8. Epub 2004/12/17. doi:
860   10.1073/pnas.0405172102. PubMed PMID: 15601777; PubMed Central PMCID: PMCPMC535801.

861   41.   van Scherpenzeel M, Conte F, Bull C, Ashikov A, Hermans E, Willems A, et al. Dynamic tracing
862   of sugar metabolism reveals the mechanisms of action of synthetic sugar analogs. Glycobiology.
863   2022;32(3):239-50. Epub 2021/12/24. doi: 10.1093/glycob/cwab106. PubMed PMID: 34939087;
864   PubMed Central PMCID: PMCPMC8966471.

865   42.   Karakus U, Pohl MO, Stertz S. Breaking the convention: Sialoglycan variants, coreceptors, and
866   alternative receptors for influenza A virus entry. J Virol. 2020;94(4). Epub 2019/11/30. doi:
867   10.1128/JVI.01357-19. PubMed PMID: 31776280; PubMed Central PMCID: PMCPMC6997770.

868   43.   Fujioka Y, Nishide S, Ose T, Suzuki T, Kato I, Fukuhara H, et al. A sialylated voltage-eependent
869   Ca(2+) channel binds hemagglutinin and mediates influenza A virus entry into mammalian cells. Cell
870   Host Microbe. 2018;23(6):809-18 e5. Epub 2018/05/22. doi: 10.1016/j.chom.2018.04.015. PubMed
871   PMID: 29779930.

872   44.   Ho JW, Hershkovitz O, Peiris M, Zilka A, Bar-Ilan A, Nal B, et al. H5-type influenza virus
873   hemagglutinin is functionally recognized by the natural killer-activating receptor NKp44. J Virol.
874   2008;82(4):2028-32. Epub 2007/12/14. doi: 10.1128/JVI.02065-07. PubMed PMID: 18077718;
875   PubMed Central PMCID: PMCPMC2258730.

876   45.   Arnon TI, Achdout H, Lieberman N, Gazit R, Gonen-Gross T, Katz G, et al. The mechanisms
877   controlling the recognition of tumor- and virus-infected cells by NKp46. Blood. 2004;103(2):664-72.
878   Epub 2003/09/25. doi: 10.1182/blood-2003-05-1716. PubMed PMID: 14504081.

879   46.   Achdout H, Meningher T, Hirsh S, Glasner A, Bar-On Y, Gur C, et al. Killing of avian and swine
880   influenza virus by natural killer cells. J Virol. 2010;84(8):3993-4001. Epub 2010/02/05. doi:
881   10.1128/JVI.02289-09. PubMed PMID: 20130050; PubMed Central PMCID: PMCPMC2849486.

882   47.   Mandelboim O, Lieberman N, Lev M, Paul L, Arnon TI, Bushkin Y, et al. Recognition of
883   haemagglutinins on virus-infected cells by NKp46 activates lysis by human NK cells. Nature.
884   2001;409(6823):1055-60. Epub 2001/03/10. doi: 10.1038/35059110. PubMed PMID: 11234016.

885   48.   Eierhoff T, Hrincius ER, Rescher U, Ludwig S, Ehrhardt C. The epidermal growth factor receptor
886   (EGFR) promotes uptake of influenza A viruses (IAV) into host cells. PLoS Pathog. 2010;6(9):e1001099.
887   Epub 2010/09/17. doi: 10.1371/journal.ppat.1001099. PubMed PMID: 20844577; PubMed Central
888   PMCID: PMCPMC2936548.

889   49.   Chan CM, Chu H, Zhang AJ, Leung LH, Sze KH, Kao RY, et al. Hemagglutinin of influenza A virus
890   binds specifically to cell surface nucleolin and plays a role in virus internalization. Virology.
891   2016;494:78-88. Epub 2016/04/17. doi: 10.1016/j.virol.2016.04.008. PubMed PMID: 27085069.

892   50.   Byrd-Leotis L, Jia N, Dutta S, Trost JF, Gao C, Cummings SF, et al. Influenza binds
893   phosphorylated glycans from human lung. Sci Adv. 2019;5(2):eaav2554. Epub 2019/02/23. doi:
894   10.1126/sciadv.aav2554. PubMed PMID: 30788437; PubMed Central PMCID: PMCPMC6374103.

895   51.   Gambaryan A, Yamnikova S, Lvov D, Tuzikov A, Chinarev A, Pazynina G, et al. Receptor
896   specificity of influenza viruses from birds and mammals: new data on involvement of the inner
897   fragments of the carbohydrate chain. Virology. 2005;334(2):276-83. Epub 2005/03/23. doi:
898   10.1016/j.virol.2005.02.003. PubMed PMID: 15780877.

899   52.   Jia N, Barclay WS, Roberts K, Yen HL, Chan RW, Lam AK, et al. Glycomic characterization of
900   respiratory tract tissues of ferrets: implications for its use in influenza virus infection studies. J Biol
901   Chem. 2014;289(41):28489-504. Epub 2014/08/20. doi: 10.1074/jbc.M114.588541. PubMed PMID:
902   25135641; PubMed Central PMCID: PMCPMC4192499.

903   53.   Walther T, Karamanska R, Chan RW, Chan MC, Jia N, Air G, et al. Glycomic analysis of human
904   respiratory tract tissues and correlation with influenza virus infection. PLoS Pathog.
905   2013;9(3):e1003223. Epub 2013/03/22. doi: 10.1371/journal.ppat.1003223. PubMed PMID:
906   23516363; PubMed Central PMCID: PMCPMC3597497.

54.	Jia N, Byrd-Leotis L, Matsumoto Y, Gao C, Wein AN, Lobby JL, et al. The human lung glycome reveals novel glycan ligands for influenza A virus. Sci Rep. 2020;10(1):5320. Epub 2020/03/27. doi: 10.1038/s41598-020-62074-z. PubMed PMID: 32210305; PubMed Central PMCID: PMCPMC7093477.

55.	Watters KE, Fellmann C, Bai HB, Ren SM, Doudna JA. Systematic discovery of natural CRISPR-Cas12a inhibitors. Science. 2018;362(6411):236-9. Epub 2018/09/08. doi: 10.1126/science.aau5138. PubMed PMID: 30190307; PubMed Central PMCID: PMCPMC6185749.

56.	Cole NB, Smith CL, Sciaky N, Terasaki M, Edidin M, Lippincott-Schwartz J. Diffusional mobility of golgi proteins in membranes of living cells. Science. 1996;273(5276):797-801. Epub 1996/08/09. doi: 10.1126/science.273.5276.797. PubMed PMID: 8670420.

57.	Canals I, Ginisty A, Quist E, Timmerman R, Fritze J, Miskinyte G, et al. Rapid and efficient induction of functional astrocytes from human pluripotent stem cells. Nat Methods. 2018;15(9):693-6. Epub 2018/08/22. doi: 10.1038/s41592-018-0103-2. PubMed PMID: 30127505.

58.	Qiu B, de Vries RJ, Caiazzo M. Direct cell reprogramming of mouse fibroblasts into functional astrocytes using lentiviral overexpression of the transcription factors NFIA, NFIB, and SOX9. Methods Mol Biol. 2021;2352:31-43. Epub 2021/07/30. doi: 10.1007/978-1-0716-1601-7_3. PubMed PMID: 34324178.

59.	Dull T, Zufferey R, Kelly M, Mandel RJ, Nguyen M, Trono D, et al. A third-generation lentivirus vector with a conditional packaging system. J Virol. 1998;72(11):8463-71. Epub 1998/10/10. doi: 10.1128/JVI.72.11.8463-8471.1998. PubMed PMID: 9765382; PubMed Central PMCID: PMCPMC110254.

60.	Perez-Riverol Y, Bai J, Bandla C, Garcia-Seisdedos D, Hewapathirana S, Kamatchinathan S, et al. The PRIDE database resources in 2022: a hub for mass spectrometry-based proteomics evidences. Nucleic Acids Res. 2022;50(D1):D543-D52. Epub 2021/11/02. doi: 10.1093/nar/gkab1038. PubMed PMID: 34723319; PubMed Central PMCID: PMCPMC8728295.

61.	de Vries RP, de Vries E, Bosch BJ, de Groot RJ, Rottier PJ, de Haan CA. The influenza A virus hemagglutinin glycosylation state affects receptor-binding specificity. Virology. 2010;403(1):17-25. Epub 2010/05/06. doi: 10.1016/j.virol.2010.03.047. PubMed PMID: 20441997.

62.	Zeng Q, Langereis MA, van Vliet AL, Huizinga EG, de Groot RJ. Structure of coronavirus hemagglutinin-esterase offers insight into corona and influenza virus evolution. Proc Natl Acad Sci U S A. 2008;105(26):9065-9. Epub 2008/06/14. doi: 10.1073/pnas.0800502105. PubMed PMID: 18550812; PubMed Central PMCID: PMCPMC2449365.

63.	Shaner NC, Lin MZ, McKeown MR, Steinbach PA, Hazelwood KL, Davidson MW, et al. Improving the photostability of bright monomeric orange and red fluorescent proteins. Nat Methods. 2008;5(6):545-51. Epub 2008/05/06. doi: 10.1038/nmeth.1209. PubMed PMID: 18454154; PubMed Central PMCID: PMCPMC2853173.

64.	Cooper CA, Gasteiger E, Packer NH. GlycoMod - a software tool for determining glycosylation compositions from mass spectrometric data. Proteomics. 2001;1(2):340-9. Epub 2001/10/30. doi: 10.1002/1615-9861(200102)1:2<340::AID-PROT340>3.0.CO;2-B. PubMed PMID: 11680880.

65.	Kärber G. Beitrag zur kollektiven Behandlung pharmakologischer Reihenversuche. Naunyn-Schmiedebergs Archiv für experimentelle Pathologie und Pharmakologie. 1931;162(4):480-3. doi: 10.1007/BF01863914.

Figures

949
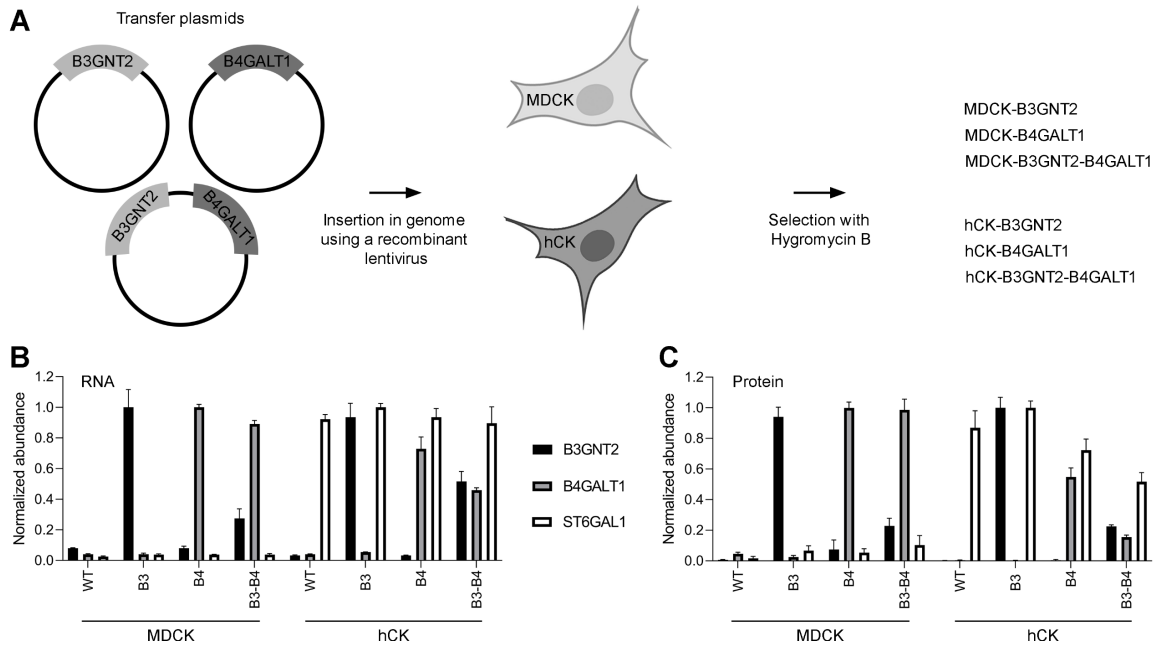
950

951 **Fig 1. Construction of MDCK and hCK cells that overexpress B3GNT2 and/or**
952 **B4GALT1**
953 (**A**) MDCK and hCK cells were modified with recombinant lentiviruses containing
954 transfer plasmids for the insertion of the *B3GNT2* and/or *B4GALT1* gene and the
955 Hygromycin B resistance gene. The knock-in cells were selected with 300 µg/ml
956 Hygromycin B. (**B**) RT-qPCR was performed with primers that anneal to both the
957 human and dog *B3GNT2*, *B4GALT1*, or *ST6GAL1* genes. The values relative to the
958 dog *GAPDH* gene were used, which were then normalized to the highest value of each
959 gene. Mean and SD (n=3) are shown. (**C**) Mass spectrometry of the B3GNT2,
960 B4GALT1, and ST6GAL1 proteins. Only peptides unique to human proteins were
961 selected. All samples were normalized against tubulin beta and then normalized to the
962 highest value of each protein. Mean and SD (n=3) are shown.

39
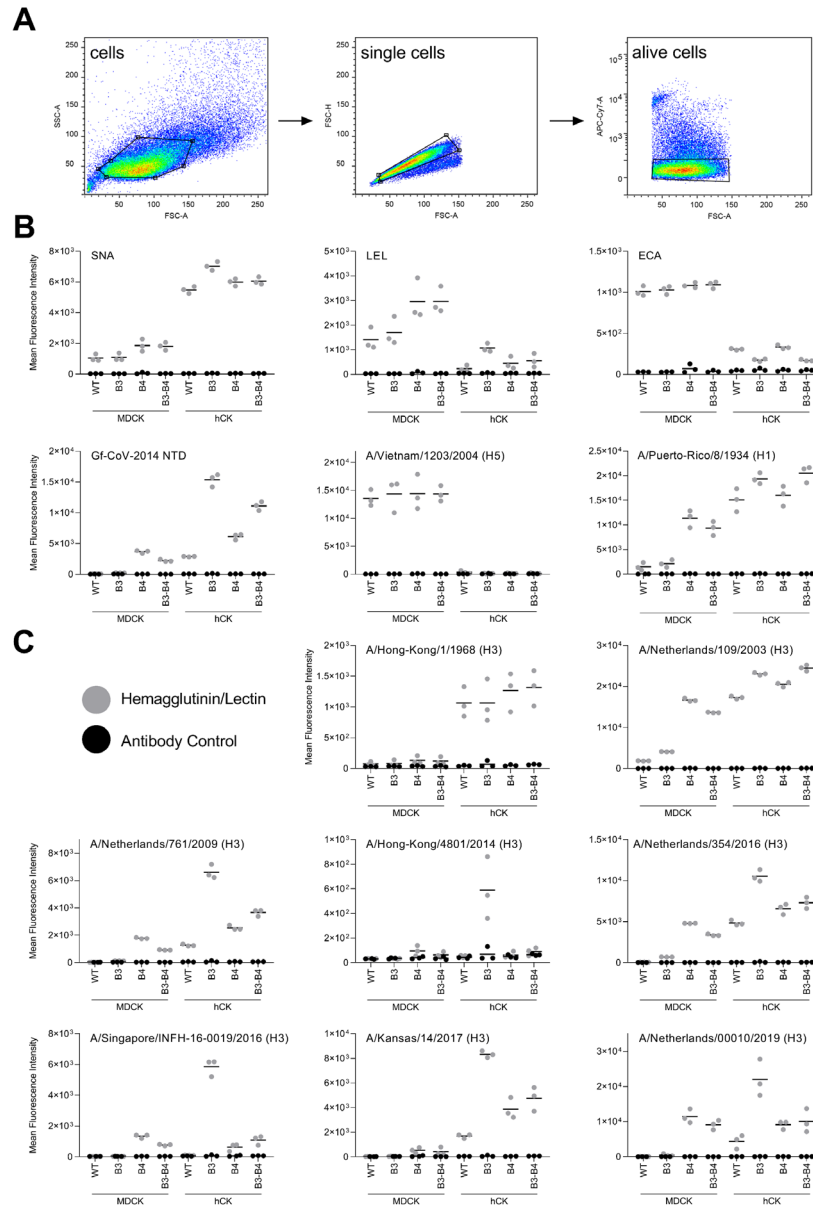
Fig 2. Flow cytometric characterization of B3GNT2/B4GALT1 knock-in MDCK and hCK cells

(**A**) The gating strategy that was used to select single, alive cells. (**B**) Flow cytometry measurements with lectins SNA (*Sambucus nigra* agglutinin, recognizes α2,6-SIA), LEL (*Lycopersicon esculentum* lectin, recognizes elongated glycans), and ECA (*Erythrina cristagalli* lectin, recognizes glycans without SIA) were performed. Furthermore, Gf-CoV-2014 NTD was used to detect elongated glycans, H5 HA of A/Vietnam/1203/2004 was used to detect α2,3-SIA, and H1 HA from A/Puerto-Rico/8/1934 was used as a standard influenza virus. Triplicate measurements were performed, of which the mean and all individual measurements are displayed. (**C**) A diverse set of H3 HAs was used to characterize the cells. Triplicate measurements were performed, of which the mean and all individual measurements are displayed. Titration curves of A/Hong-Kong/1/1968, A/Netherlands/109/2003, and A/Singapore/INFH-16-0019/2016 are shown in Fig. S2. Flow cytometric experiments with neuraminidase treatment of the cells are shown in Fig. S3

40

979
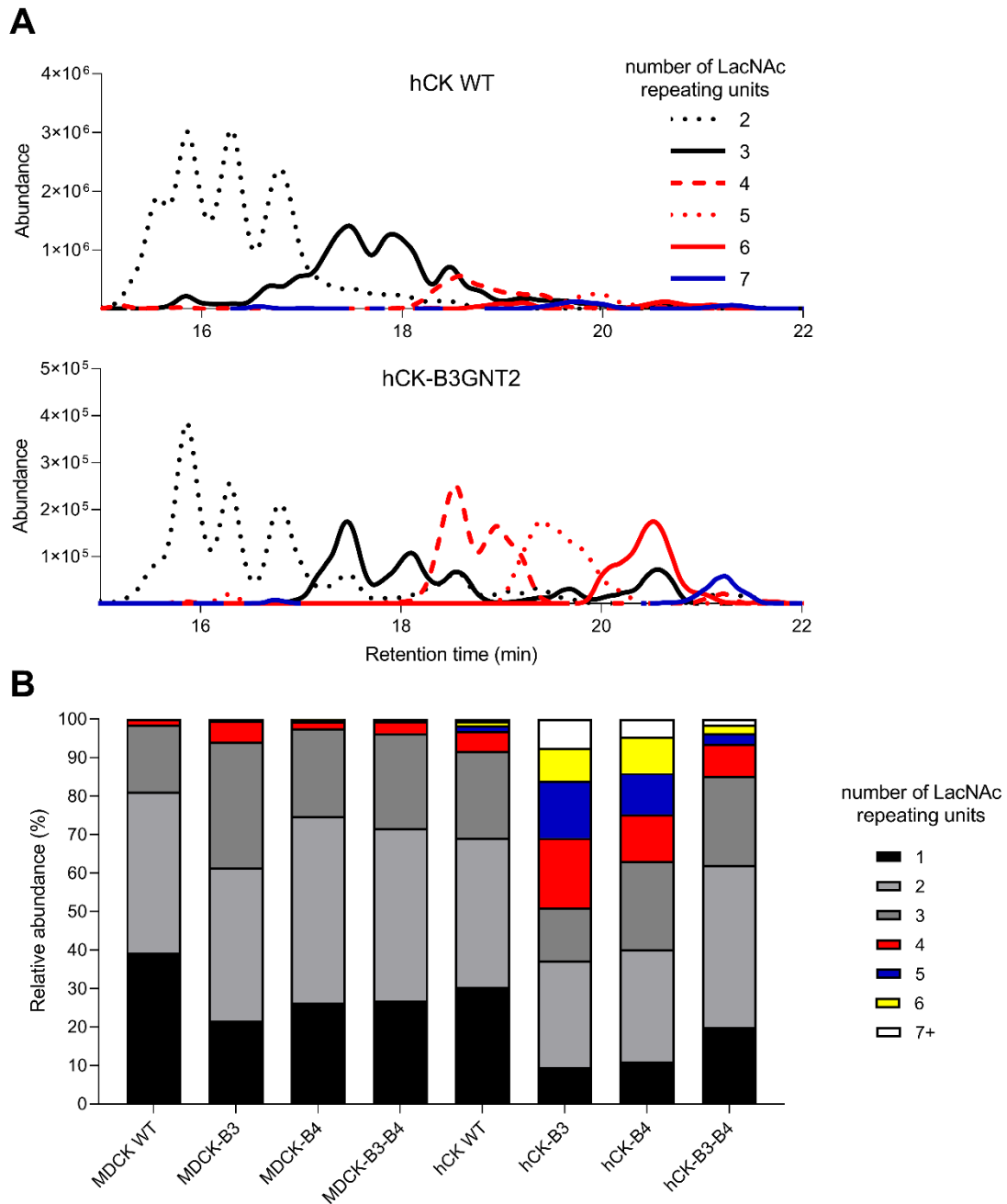
**Fig 3. *N*-glycan analysis of WT and B3GNT2/B4GALT1 knock-in MDCK and hCK cells using mass spectrometry**

The *N*-glycans from WT and B3GNT2/B4GALT1 knock-in MDCK and hCK cells were measured using mass spectrometry. (**A**) Chromatograms of hCK WT and hCK-B3GNT2 cells were constructed for the glycans with at least two and at most seven LacNAc repeating units. The extracted-ion-counts for the ten most abundant glycan features per LacNAc repeating unit group were summed to yield a chromatogram. (**B**) The *N*-glycans with at least one LacNAc repeating unit were analyzed for the number of LacNAc repeating units present and the relative abundance was calculated. Further analysis is presented in Figure S4. Full glycan feature lists for each cell line are presented in Table S1-8.

991
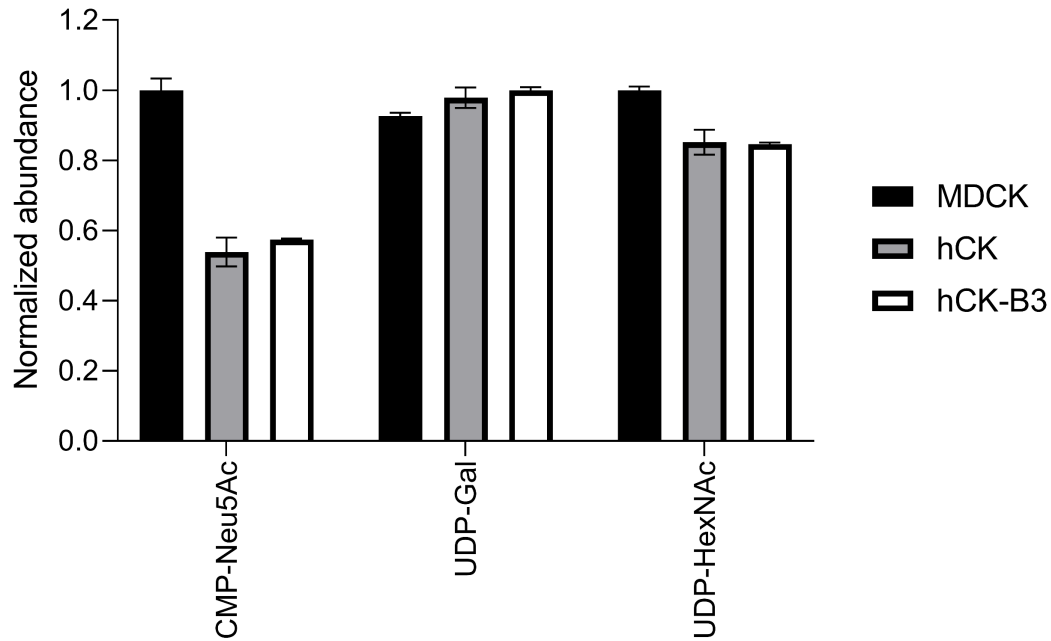
Fig 4. Sugar nucleotide analysis of MDCK, hCK, and hCK-B3GNT2 cells
The sugar nucleotides in the lysate of MDCK, hCK, and hCK-B3GNT2 cells were analyzed by mass spectrometry (n=2). The normalized abundance of CMP-Neu5Ac, UDP-Gal, and UDP-HexNAc are shown. Normalization was performed on the cell line with the highest amount of each sugar nucleotide. Detailed information about all measured sugar nucleotides is presented in Fig. S4.

998
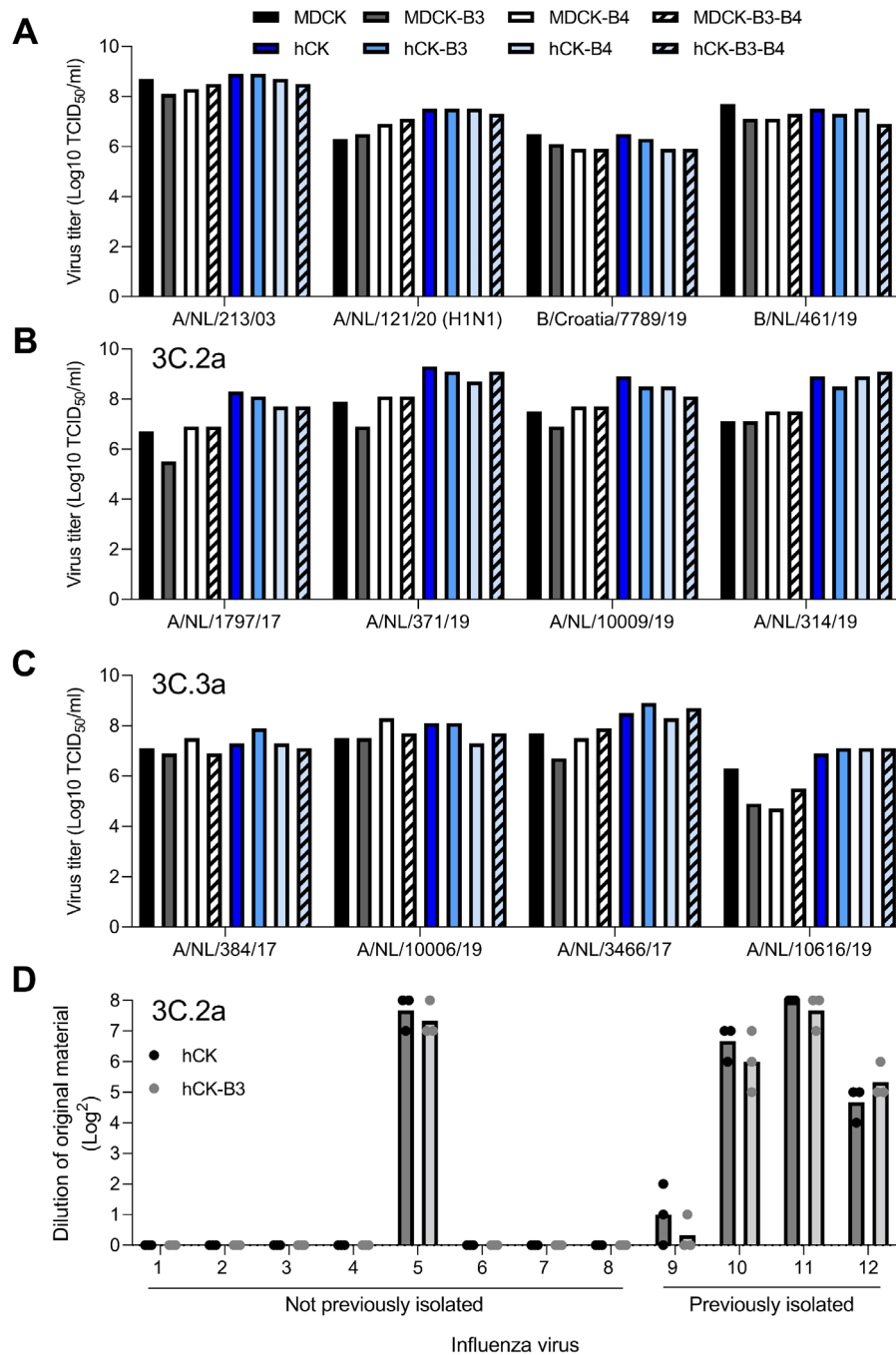
Fig 5. Influenza virus inoculation of B3GNT2 and B4GALT1 knock-in MDCK and hCK cells

End-point titrations with four control viruses and eight recent H3N2 IAVs (details in Table 3) were performed, of which (**A**) four control viruses, (**B**) four 3C.2a viruses, and (**C**) four 3C.3a viruses. Infectious titers were determined either using a hemagglutination assay (**A**) or a nucleoprotein staining (**B**, **C**) when a hemagglutination assay was not possible. (**D**) An infection study using hCK and hCK-B3GNT2 cells with a twofold dilution of twelve H3N2 IAVs from the 3C.2a clade (details in Table 4) which could previously either not be isolated in hCK cells (#1-8) or could be isolated in hCK cells (#9-12) was performed. Infection was assessed by the presence of cytopathic effects. Individual and mean values are shown.

1010 **Supplementary figures**
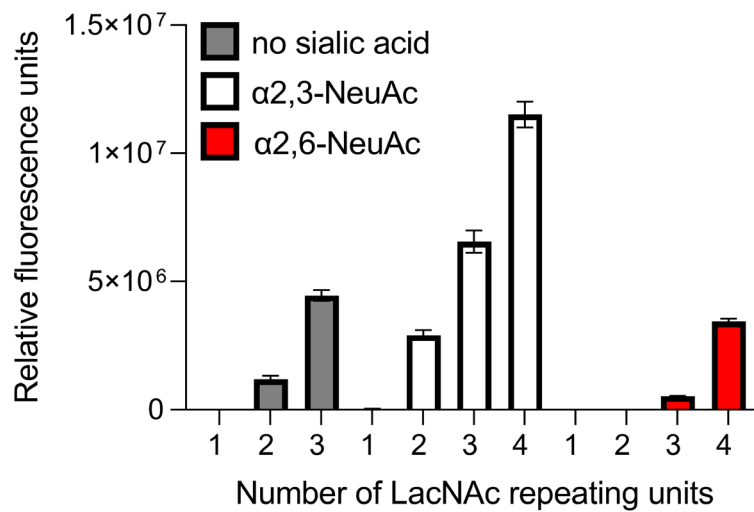
1011

1012 **Fig S1. Binding specificity of *Lycopersicon esculentum* lectin on the glycan**
1013 **microarray**
1014 The binding of the *Lycopersicon esculentum* lectin (LEL) to symmetric bi-antennary *N*-
1015 glycans with 1, 2, 3, or 4 consecutive LacNAc repeating units terminating in no sialic
1016 acid, α2,3-linked NeuAc, or α2,6-linked NeuAc was investigated. Six replicates were
1017 performed simultaneously, after which the highest and lowest replicates were
1018 removed, and the mean and standard deviation were calculated over the four
1019 remaining replicates. The glycan array was performed as described earlier [35].
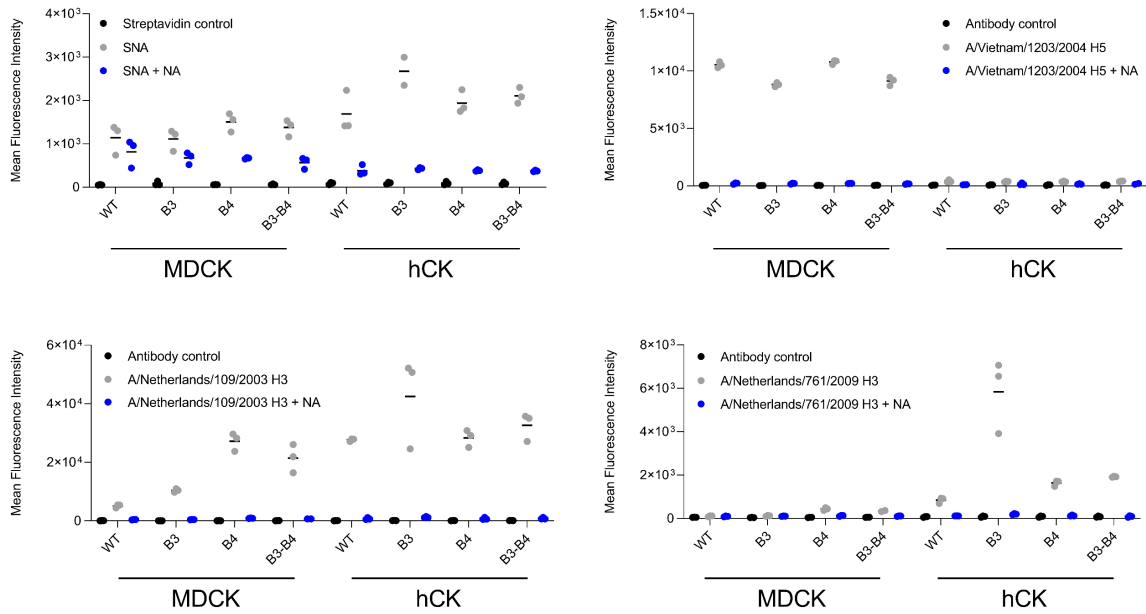
1020

Fig S2. Flow cytometry with neuraminidase-treated B3GNT2/B4GALT1 knock-in MDCK and hCK cells

Binding of the lectin SNA and HAs A/Vietnam/1203/2004 H5, A/Netherlands/109/2003 H3, and A/Netherlands/761/2009 H3 with and without neuraminidase (NA) were measured using flow cytometry. The gating strategy as indicated in Fig. 2A was used. Triplicate measurements were performed and the mean and all individual measurements are shown.
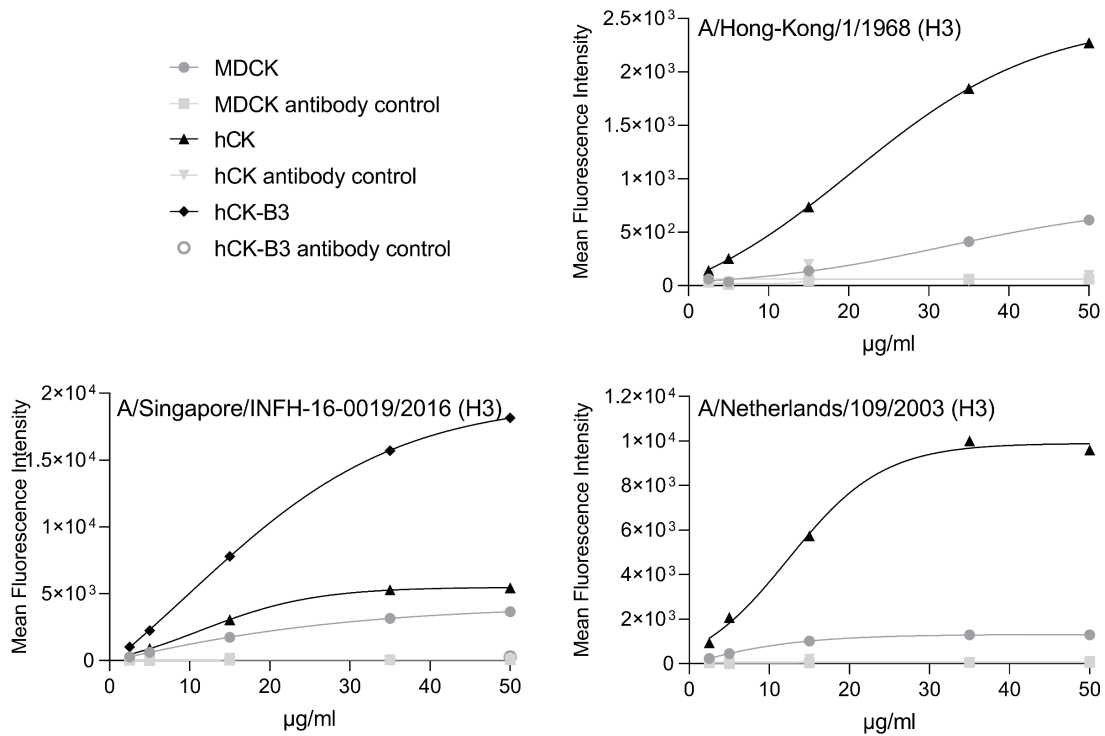
1028

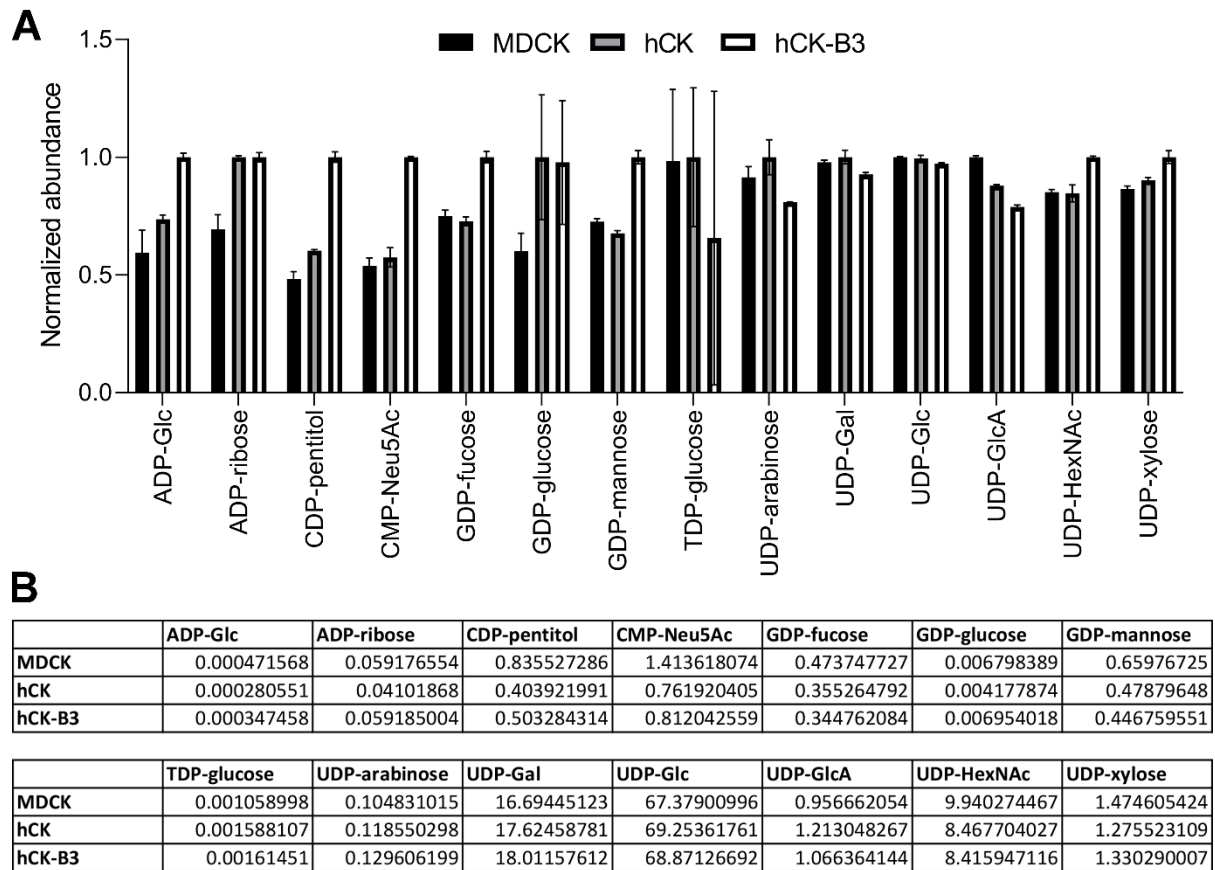**Fig S3. Titration of influenza hemagglutinins in flow cytometry**
Flow cytometric titrations of the H3 HAs of A/Hong-Kong/1/1968, A/Singapore/INFH-16-0019/2016, and A/Netherlands/109/2003 in MDCK and hCK cells, including controls in the presence of just precomplexing controls were performed. For A/Singapore/INFH-16-0019/2016, also hCK-B3GNT2 cells were used. The gating strategy as described in Fig. 2A was used.
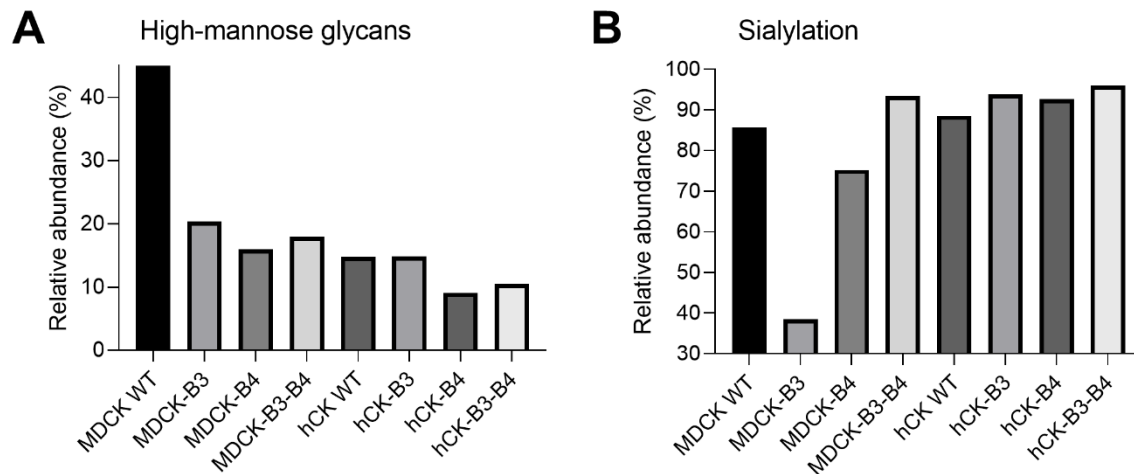
Fig S4. Relative abundance of high-mannose glycans and sialylation on WT and B3GNT2/B4GALT1 knock-in MDCK and hCK cells

The *N*-glycans from WT and B3GNT2/B4GALT1 knock-in MDCK and hCK cells were measured using mass spectrometry. (**A**) The relative abundance of high-mannose glycans was calculated as a percentage of all detected *N*-glycans (see Table S1-8). (**B**) The relative abundance of glycans (30-100%) with at least one SIA was calculated as a percentage of the total abundance of glycans with at least one LacNAc repeating unit (the glycans shown in Fig. 3B).

A

B

	ADP-Glc	ADP-ribose	CDP-pentitol	CMP-Neu5Ac	GDP-fucose	GDP-glucose	GDP-mannose
MDCK	0.000471568	0.059176554	0.835527286	1.413618074	0.473747727	0.006798389	0.65976725
hCK	0.000280551	0.04101868	0.403921991	0.761920405	0.355264792	0.004177874	0.47879648
hCK-B3	0.000347458	0.059185004	0.503284314	0.812042559	0.344762084	0.006954018	0.446759551

	TDP-glucose	UDP-arabinose	UDP-Gal	UDP-Glc	UDP-GlcA	UDP-HexNAc	UDP-xylose
MDCK	0.001058998	0.104831015	16.69445123	67.37900996	0.956662054	9.940274467	1.474605424
hCK	0.001588107	0.118550298	17.62458781	69.25361761	1.213048267	8.467704027	1.275523109
hCK-B3	0.00161451	0.129606199	18.01157612	68.87126692	1.066364144	8.415947116	1.330290007

1044

1045 **Fig S5. Sugar nucleotide analysis of MDCK, hCK, and hCK-B3GNT2 cells**
1046 The sugar nucleotides in the lysate of MDCK, hCK, and hCK-B3GNT2 cells were
1047 analyzed by mass spectrometry (n=2). (**A**) The normalized abundance of all measured
1048 sugar nucleotides is shown. Normalization was performed on the cell line with the
1049 highest amount of each sugar nucleotide. (**B**) Details of all analyzed sugar nucleotides,
1050 normalized over the sum of all measured nucleotide sugars.